To the Graduate Council:

I am submitting herewith a thesis written by Philip L. Andrew entitled "A Computational Fluid Dynamic Method for Rotating Stall in a Single Stage Axial Compressor." I have examined the final copy of this thesis for form and content and recommend that it be accepted in partial fulfillment of the requirements for the degree of Master of Science, with a major in Mechanical Engineering.

John E. Caruthers

John E. Caruthers, Major Professor

We have read this thesis
and recommend its acceptance:

J C Reddy

Accepted for the Council:

CW Minkel

Vice Provost
and Dean of The Graduate School

STATEMENT OF PERMISSION TO USE

In presenting this thesis in partial fulfillment of the requirements for a Master's degree at The University of Tennessee, Knoxville, I agree that the Library shall make it available to borrowers under rules of the Library. Brief quotations from this thesis are allowable without special permission, provided that accurate acknowledgment of source is made.

Permission for extensive quotation from or reproduction of this thesis may be granted by my major professor, or in his absence, by the Head of Interlibrary Services when, in the opinion of either, the proposed use of the material is for scholarly purposes. Any copying or use of the material in this thesis for financial gain shall not be allowed without my written permission.

Signature Philip L. Andrew

Date 19 November 1985

A COMPUTATIONAL FLUID DYNAMIC METHOD FOR ROTATING STALL IN A SINGLE STAGE AXIAL COMPRESSOR

A Thesis

Presented for the

Master of Science

Degree

The University of Tennessee, Knoxville

Philip L. Andrew

December 1985

ACKNOWLEDGMENTS

This investigation was sponsored by the United States Air Force under contract number R02-400374 and under the auspices of Sverdrup Technology Incorporated, an operating contractor of the Arnold Engineering Development Center, Tullahoma, Tennessee.

The author would like to express his sincere appreciation to the many individuals whose contributions have assisted in the completion of this effort. Firstly, he would like to thank the Sverdrup Corporation for sponsoring his Graduate Research Assistantship and especially Dr. Ralph Jones of the Propulsion Analysis group who managed the contract and who provided his valuable and timely assistance. Secondly, the author wishes to thank the individuals at the Technical University of Aachen, West Germany, whose computing facilities and other assistance was instrumental in the latter phase of the project. The author would like to gratefully acknowledge the Unsteady Loss and Deviation Models as the creation of Dr. John E. Caruthers of The University of Tennessee, whose friendship and guidance greatly enhanced the quality of this author's graduate education. The assistance of the remaining members of the author's committee, Dr. M. Kurosaka and Dr. K. C. Reddy was also appreciated. Next, the author would like to thank Mr. William N. Dalton, a friend and mentor, who often lent valuable insight into this problem and other technical discussions. Last but in no way least, the author is greatly indebted to Mrs. Kathy Hice for her cheerful clerical assistance in the preparation of the thesis draft and to Mrs. Ruth White for her conscientious typing of the final copy.

ABSTRACT

This thesis elucidates the development of a computer program to model the unsteady phenomenon of propagating (or rotating) stall in a single stage, axial compressor. This development involved the modification of an existing computer program designated as ARO-1 which was written by J. L. Jacocks and K. R. Kneile of the Arnold Engineering Development Center, Tullahoma, Tennessee. [1]* This code takes the finite volume approach in solving the three dimensional, unsteady Euler equations in cartesian coordinates via the explicit predictor-corrector algorithm credited to MacCormack. [2]

Using this code as a starting point, the compressor is herein modeled in two dimensions, axial and circumferential, with the inertial grid "unwrapped" from about the compressor annulus to form a rectangular cartesian coordinate system. In modeling the compressor blading, the approach taken is essentially a semi-actuator disc method wherein two of the conservation partial differential equations are replaced by two algebraic constraint equations. Since the Euler equations inherently fail to account for the viscous phenomenon of rotating stall, an unsteady cascade loss model and an unsteady cascade deviation angle model were implemented.

---

*Numbers in square brackets refer to references given at the end of this thesis.

NOMENCLATURE

Roman Symbols

A . . Flow area (ft^2)

C . . Sonic velocity (ft/sec)

C_x . . Axial flow velocity

C_p . . Specific heat at constant pressure (Btu/lbm-°R)

C_v . . Specific heat at constant volume (Btu/lbm-°R)

e . . Specific energy (Btu/lbm)

E_2 . . Energy variable as defined in text (lbf/ft^2)

F . . Tensor of conservation variables as defined in text

g . . Gravitational constant

G . . Vector of conservation variables as defined in text

h . . Specific enthalpy

H . . total enthalpy

imp . . Impulse function

i . . Incidence angle in degrees

$\hat{j}$ . . Unit vector in tangential direction

k . . Thermal conductivity coefficient

M . . Mach number

$\hat{n}$ . . Unit normal vector

N . . Time level

p . . Pressure (lbf/ft^2)

q . . Velocity vector

Q . . Corrected flowrate

R . . Gas constant for air (ft-lbf/lbm°R)

S . . Entropy (ft-lbf/lbm°R)

S . . Flux surface

t . . Time (sec)

T . . Temperature (°R)

u . . Axial flow velocity (ft/sec)

v . . Tangential flow velocity (ft/sec)

$\forall$ . . Volume (ft^3)

w . . Specific work

W . . Work

ws . . Wheel speed

W_s . . Source term

x . . Axial direction

y . . Tangential direction

z . . Radial direction

Greek Symbols

β . . Relative flow angle

γ . . Ratio of specific heats

δ . . Deviation angle

θ . . Absolute flow angle

ρ . . Density (lbm/ft^3)

ϕ . . Flow coefficient

ψ . . Nondimensional pressure rise

$\bar{\omega}$ . . Loss coefficient

Subscripts

i . . Inflow

v . . Unit volume basis

ti . . Total inlet

m . . Pertains to blade metal angle

o . . Stagnation property

rf . . Relative flow

ts . . Total to static

TABLE OF CONTENTS

LIST OF FIGURES

FIGURE PAGE

INTRODUCTION

Gas Turbine Engine Stability

The attainment of acceptable performance in a modern gas turbine engine pivots upon the aerodynamically stable operation of the compressor at all points of the intended operating range. The line demarcating stable and unstable operation on a compressor performance map (a plot of total pressure rise across the compressor versus corrected flowrate) (Figure 1), is known as the stability limit line or, the surge line.

An operating point below the surge line is stable wherein the compressor delivers an intended pressure rise at a given flow rate. In contrast, operation above the surge line results in compressor surge, an unstable mode of operation wherein the engine's ability to produce thrust is severely degraded. Prior to entering the surge regime (or, sometimes during a surge cycle) a compressor may experience a rotating stall mode of operation which, once instigated, may become a new stable operating condition.

The stability limit line is unique to a given compressor design. It is typically derived from steady-state (and a modicum of unsteady) experimental data in addition to empirical corrections and correlations. During the operation of the compressor system, the stability limit line changes as a function of fluctuations and

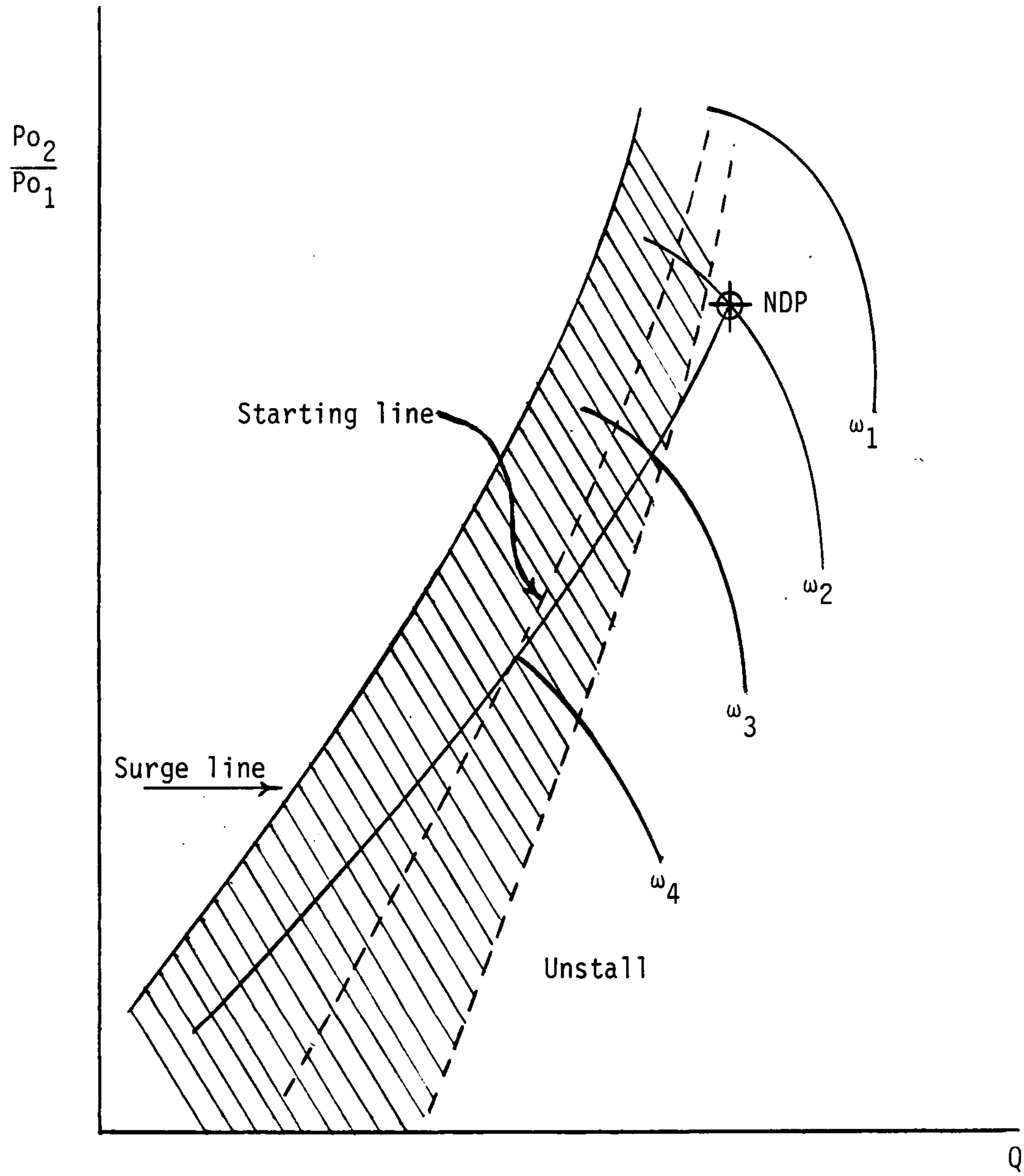

Figure 1. Compressor Performance Map.

distortions of the inlet flow and also due to other unsteady phenomena. The stall line is analogously affected. Thus mathematical models are employed in order to emulate the operation of compressor systems under many more operating conditions than are practical to investigate experimentally.

Rotating Stall vis-a-vis Surge

As the flow through an axial compressor is progressively throttled from the design point, the initially steady, axisymmetric flow pattern becomes unstable. This instability is manifest in the instigation of the unsteady and highly non-linear phenomena of surge and/or rotating stall.

Surge, as depicted in Figure 2, is characterized by a large amplitude oscillation of the total annulus-averaged flow through the compressor. In contrast, rotating stall as shown in Figure 3 is characterized by one-to-several cells of severely retarded flow that rotate about the compressor circumference. In addition, the frequencies of axial flow direction reversal associated with surge are typically an order of magnitude less than those frequencies associated with the propagation of rotating stall cells.

Stall Cell Propagation

The propagation of a stall cell may be elucidated by considering the effect of suddenly throttling a compressor that is initially operating in a steady state. Since the inertia of the rotating components is high, the speed of the rotor remains essentially constant

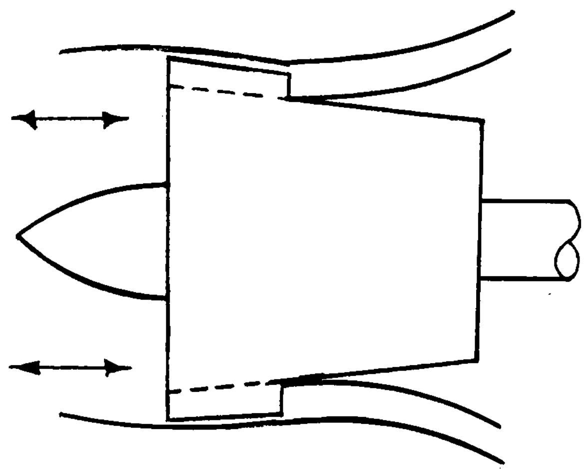

Figure 2. Surge - Axially Oscillating Flow.

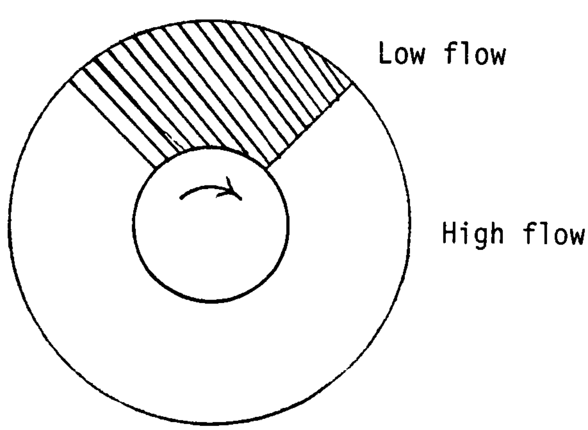

Figure 3. Rotating Stall - Circumferentially Nonuniform Flow.

for the first part of the transient. Concurrently, the flow rate decreases from the steady-state value, causing the angle of incidence (and thus the blade loading) to increase. Subsequently, one or more blades may stall, the flow separating from the blade, thus creating effectively a blockage of the blade passage as shown in Figure 4. The resulting decrease in flow area causes an increase in the angle of incidence of blade A of Figure 4 while decreasing the angle of incidence of blade C. As a result, blade A will tend to stall while blade B will tend to unstall, thus propagating the stall cell along the compressor circumference.

Hysteresis Phenomena Associated with Rotating Stall

Once the rotating stall mode has been instigated, it may not be possible to return to the unstalled operating point merely by re-opening the throttle. This hysteresis may be illustrated by a second type of compressor performance map as in Figures 5a and 5b, plots of load coefficient versus flow coefficient. These figures elucidate two types of behavior at the stall limit known as progressive stall and full span stall.

Progressive Stall

Referring to Figure 5a, progressive stall is so named because there exists a gradual decrease in delivery pressure as the compressor is throttled further from the stall limit at point A. At this point, there typically develop one or more cells of severely retarded flow that do not encompass the entire flow annulus height, the cells

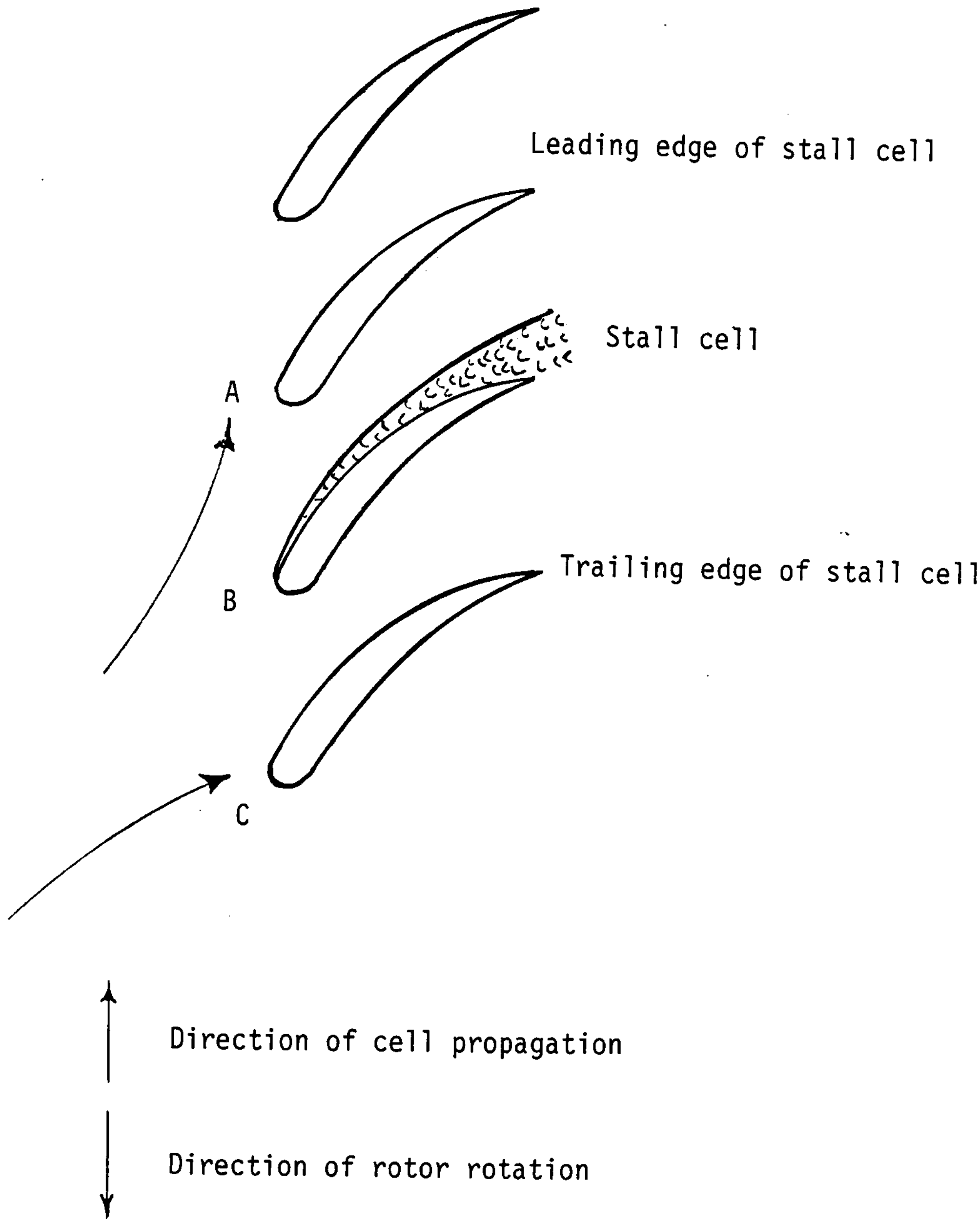

Figure 4. Stall Cell Propagation.

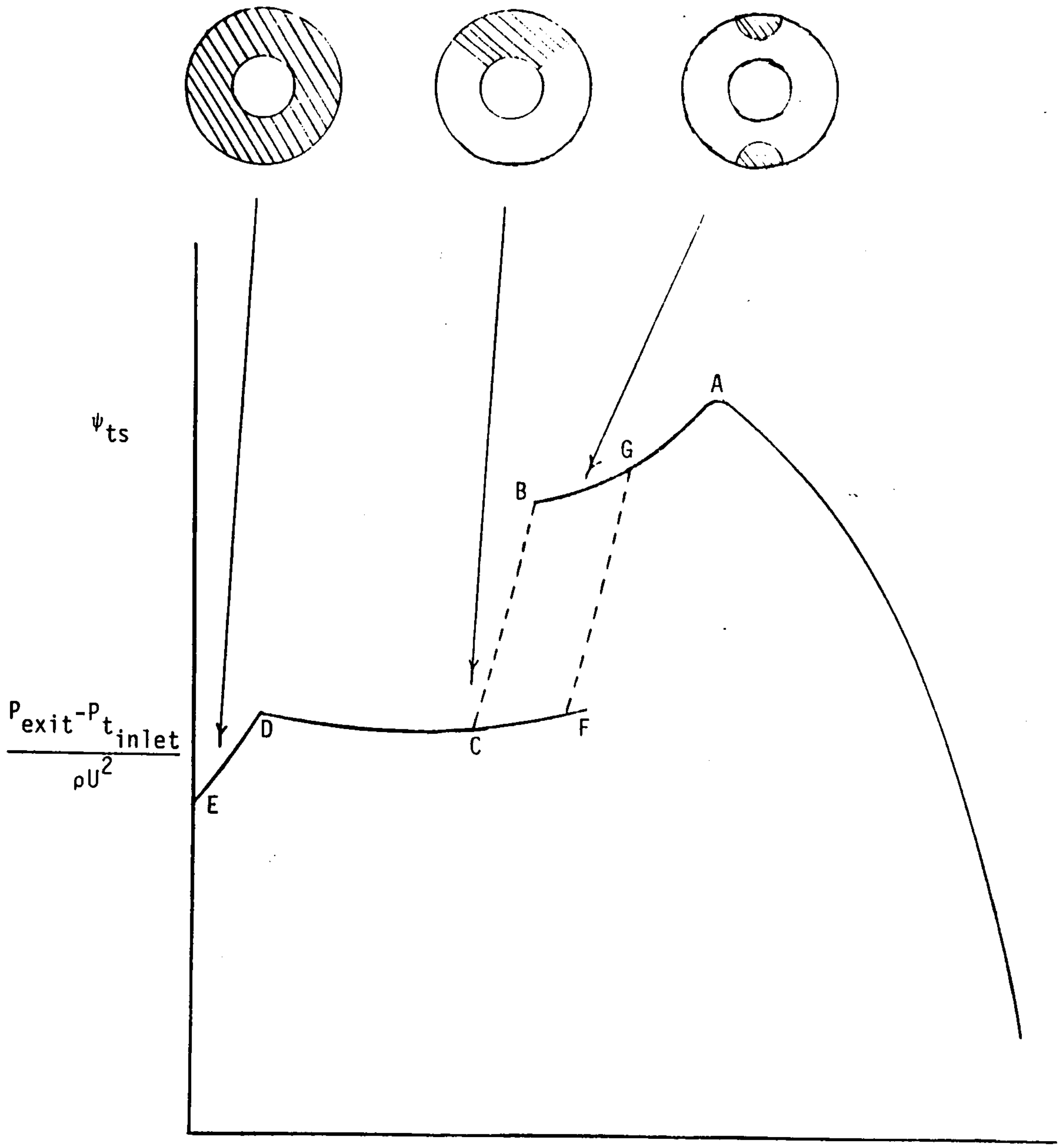

Figure 5a. Progressive Stall Characteristic (Part Span Stall).

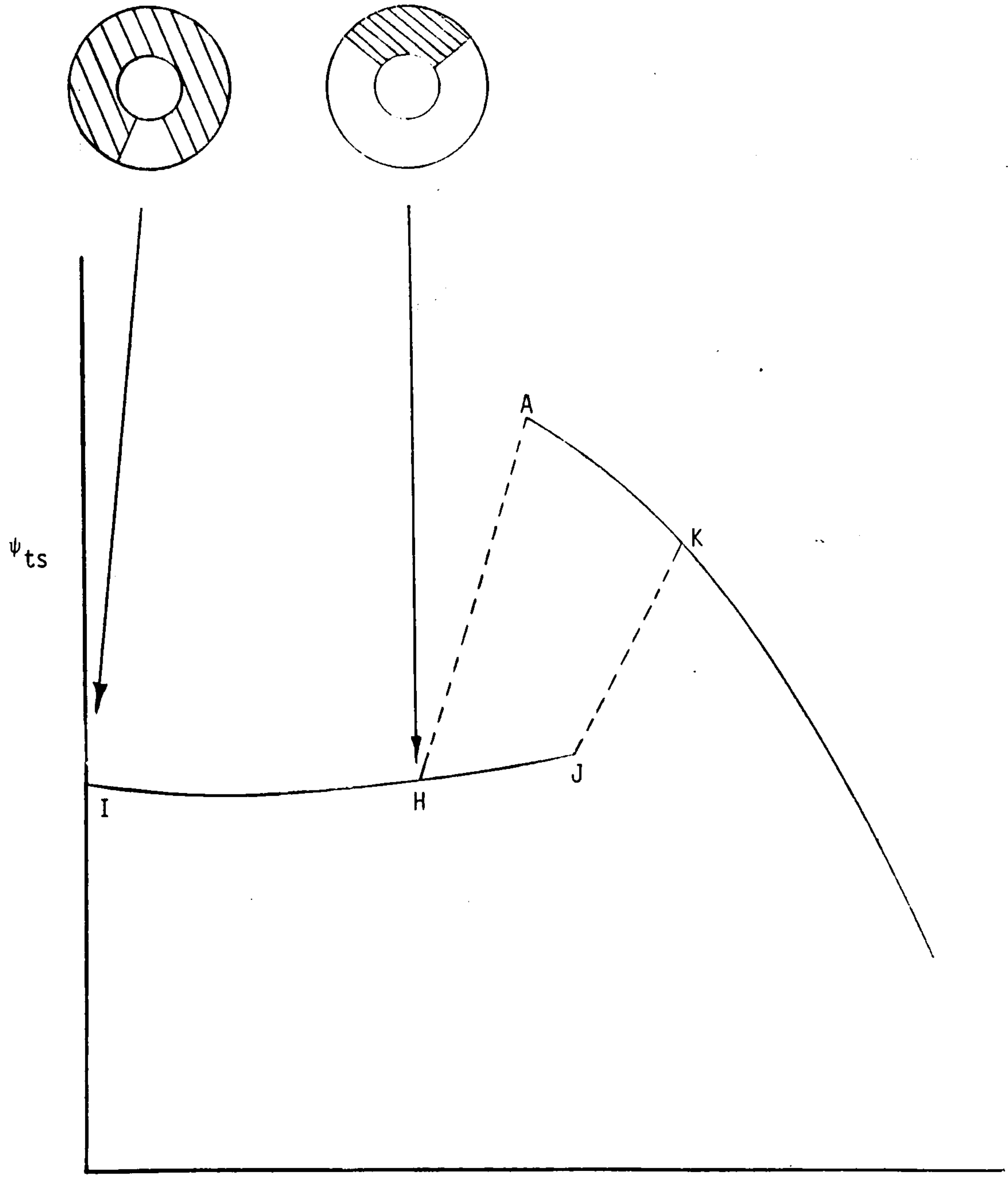

Figure 5b. Abrupt Stall Characteristic
(Full Span Stall).

forming at either the tip or the hub. Upon further throttling from the stall limit, the decrease in flow rate corresponds to a gradual decrease in delivery pressure rise, depicted as line segment A-B in the figure. Upon continued throttling from B to C, the performance curve may evidence a significant discontinuity in mass flow rate and pressure rise. This change is associated with a transition in stall cell type wherein the several cells conglomerate into a single cell which may occupy a sizable fraction of the compressor circumference and may also extend over the full annulus height. These two flow types (at points B and C) are termed part span stall and full span stall respectively. Still further throttling from point C to point D results in a relatively constant delivery pressure rise concurrent with a growth in stall cell size. As the mass flow rate approaches zero from point D to point E, the stall cell may occupy the flow annulus entirely, returning the flow to an axisymmetric condition, and corresponding to a slight further reduction in pressure rise.

If one were to now re-open the throttle gradually, he would find that the mass flow rate at which the compressor left the full span stall regime, point F, is different than that at which it entered (point C). This illustrates the hysteresis-like nature of the rotating stall phenomenon. The hysteresis area enclosed by points B-C-F-G may comprise a significant portion of the compressor map, especially in the case of high performance and multistage machines. However, the hysteresis phenomenon associated with the onset and cessation of part span stall is usually of negligible importance relative to that associated with full span stall.

Full Span Stall

The development of full span stall, as illustrated by Figure 5b, may be instigated by a similar throttling process. In contrast to part span stall however, the discontinuity in flow rate and pressure rise occurs at the stall limit. As indicated in the figure, the change in these quantities as the operating point shifts from point A to point H is associated with the compressor transitioning into a single, full span stall. This stall cell continues to grow upon further throttling though it may not occupy the entire annulus even at zero mass flow through the compressor. As shown, the delivered pressure rise remains relatively constant as the operating point travels from H to I. Upon re-opening the throttle, it is evident from the figure that a substantial hysteresis exists between the onset and cessation of full span stall.

Rotating Stall Cell Structure

The propagation of stall cells is a highly localized, non-linear, and unsteady phenomenon. As previously discussed, the stall cell at any given time may affect only a fraction of the blade height. In addition, the stall cell may sometimes influence only a few stages of a multi-stage compressor. Detailed experimental investigations by researchers such as Day, Cumpsty, Greitzer et al. have served to characterize the stall cell not as "dead region" (analogous to the wake behind a bluff body, for example) as was previously presumed, but rather as a highly active locality. Though the axial velocity through the stall cell may be taken as zero, the tangential velocity in the cell is high, exceeding the blade speed in some instances. In addition, fluid continually enters the cell from the unstalled region through the "trailing edge" and leaves through the cell "leading edge" as shown in Figure 6. This can be attributed to the fact that stall cell speeds are usually less than "half the blade speed, while the mean swirl velocity of a 50% reaction compressor is half the blade speed, so that fluid particles in the unstalled region are always 'overtaking' the stall cell in the circumferential direction." [3]

Causes and Influences of Rotating Stall

In addition to throttling, several other methods of creating an unstable flow in a compressor exist. Among these are distortions in the inlet conditions such as a non-uniform total pressure or total temperature field. The former maldistribution may arise, for example, due to the "S" ducting preceding an engine installed in an aircraft fuselage. The latter non-uniformity can arise in military applications wherein the aircraft engine may ingest a portion of the combustion products of a munition it is launching. Another major instigator of rotating stall is the transient operating condition such as engine acceleration, deceleration and the lighting of afterburners.

During operation in the rotating stall flow regime, the compressor delivers a globally-reduced pressure rise and mass flow rate and additionally evidences a decrease in efficiency to as low as twenty percent. (Actually, the pressure rise across the unstalled

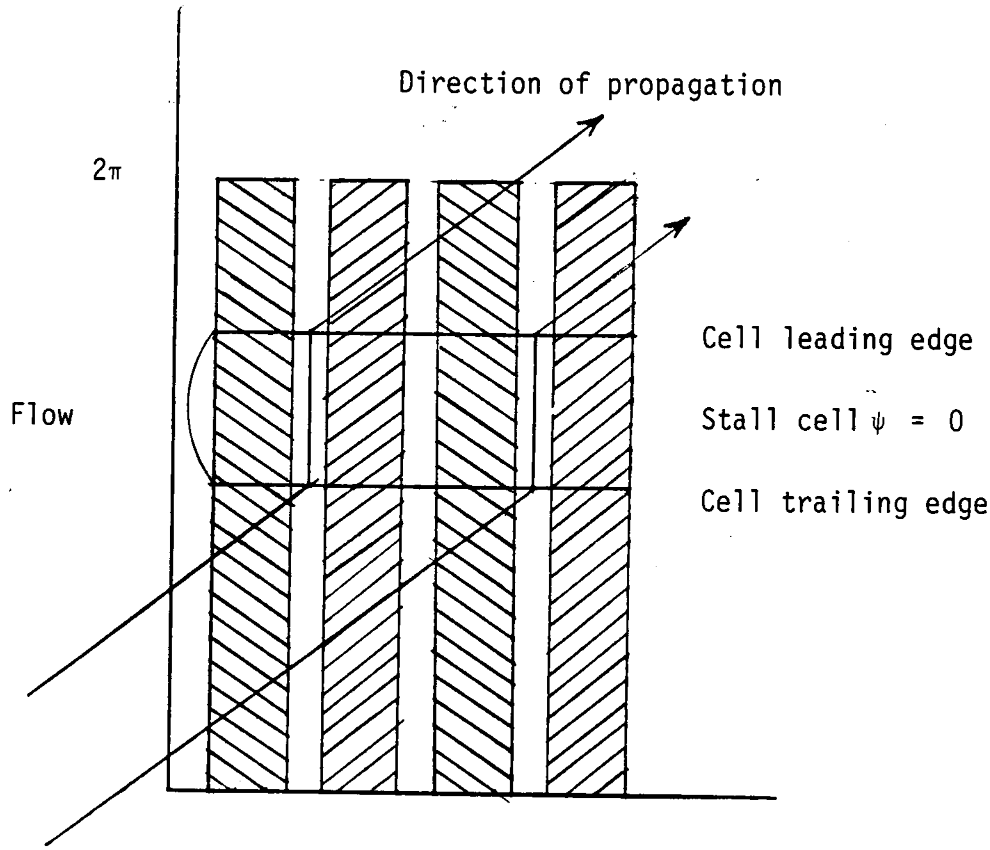

Figure 6. Stall Cell Structure.

portion of the compressor is quite normal with only the pressure ratio across the stalled portion reduced--hence the advent of so-called "parallel" compressor models found in the literature.) Since this drop in mass flow rate is not in general compensated for by an appropriate decrease in fuel flow rate, the fuel/air mixture becomes much closer to stochiometric, resulting in overtemperature in the first turbine stage or, possibly, a "flame out."

Rotating, or propagating stall also has structural dynamic implications. Since the stall cells always travel at something less than the rotor speed, the blading sees an unsteady loading and unloading due to their passage through stalled and unstalled regions. This aerodynamic forcing function may lead to an eventual fatigue failure. A more immediate failure may occur if these aerodynamic oscillations coincide with the natural frequency of one of the rotor assemblies.

Rotating stall has a further influence in terms of the starting procedure of a gas turbine engine. The starting line of a high rotational speed or a high performance compressor (i.e., those having a rather narrow performance map) will lie primarily in the rotating stall area (if there is one). This situation may prevent the attainment of even nominal design performance or it may dictate the use of a starting line not suitable for a large variety of axial compressors.

CHAPTER I

PREVIOUS INVESTIGATIONS OF ROTATING STALL

Emmons [4] et al. was the first to consider the phenomenon of rotating stall nearly thirty years ago. Though numerous theoretical and experimental investigations of the topic have been carried out in the intervening years, a comprehensive understanding of the involved fluid mechanical mechanisms remains elusive. Mathematical approaches are hindered by the difficulties associated with modeling such an unsteady, three dimensional, highly non-linear event. Experimental investigations have been retarded by the lack of the availability of suitable data acquisition techniques required to quantify the physical details of the flow within the stalled compressor.

The early experimental work generally sought to ascertain such features of the phenomenon as the number of stall cells and their angular propagation speed. More recently, Day et al. [5], Day and Cumpsty [6], and Lakhwani and Marsh [7], for example, have sought to experimentally quantify the influence of such design variables as C_x/U, the hub-tip ratio and the number of stages on the performance of the compressor operating in the propagating stall regime. This includes such quantities as the delivery pressure that one can expect in addition to the size of the hysteresis between the onset and cessation of stalled operation. This experimental work has also been useful in providing the empirical constants required in theoretical analyses.

Significant progress has been made in the development of mathematical models pertaining to propagating stall. Early models proposed by such investigators as Sears, Marble, Emmons, Stenning, and Kriebel [8], all employed linearized blade row characteristics and linearized flow equations to describe the mean flow fields upstream and down stream of the blade row for given flow conditions. If the time response of the flow was considered, it was approximated as the response of a first order system resulting in the use of a time constant. These linearized models predictably failed to emulate one or more of the important qualities of rotating stall such as the inception point, propagation speed or the number and extent of the cells. Subsequent improved models embodied nonlinear blade row characteristics, nonlinear flow equations and experimentally-determined time dependence for rotor response. Nagano and Takata [9] proposed the first such modern nonlinear stall model in 1972, solving the resulting finite difference equations on a digital computer. Concurrently, Adamcyzk [10] applied an analogous approach to determine the unsteady fluid dynamic response of an axial flow compressor stage to a distorted inlet flow.

The semi actuator disk concept was embodied in both the Nagano-Takata and the Adamczyk models. In it, the compressor is represented as a row of blades having a finite chord and an infinitesimal pitch. To describe the behavior of the semi actuator disc, these models used the characteristics of total pressure loss and turning angle as measured in stationary, two dimensional cascades. These recent models, through their inclusion of nonlinear flow equations and nonlinear blade characteristics, represent important progress in modeling rotating stall. However, they also continue to assume that the response of the blade row characteristics to changes in the inlet flow conditions is first order. Thus, they necessitate the inclusion of a time constant to be employed in the calculation of the instantaneous blade row characteristics during the unsteady flow.

The purpose of the present investigation was to develop a mathematical model to simulate the performance of a single stage, axial compressor as its operating point traveled from an unstalled condition through the stall limit. The intent was to not only predict the inception of the instability but also to ascertain the qualitative performance of the compressor during operation in the stalled flow regime. Due to the two-dimensionality of this model, only a full-span stall can be anticipated. No attempt has been made to account for the occurrence of compressor surge.

CHAPTER II

THE COMPRESSOR MODEL

The basic premise of the compressor model was to employ two solution methodologies. One solution procedure amounts to a replacement of the rotor and stator blading with a continuum model which incorporates in the static limit the steady performance of the blades. A second solution methodology solves the flowfield in the duct flow regions which surround the blade row model region. This latter solution procedure shall be presently outlined.

Flow Computation Exterior to the Compressor Cascades

The compressor model flow field was discretized as depicted in Figure 7. Areas A and C represent the duct flow regions preceding and succeeding the compressor stage. The regions R, G and S represent the rotor, the rotor/stator gap and the stator respectively. This domain was discretized uniformly in both the y (tangential or circumferential) and x (axial) directions, using an inertial rectangular cartesian coordinate system. Five axial nodes were allotted to each blade row and two nodes were placed in the rotor/stator gap. In the duct flow and the gap regions, the unsteady Euler equations were solved via the finite volume approach and the explicit predictor-corrector algorithm of MacCormack. [2] The ARO-1 code [1] was employed in its original form to solve the flow field in these duct flow regions.

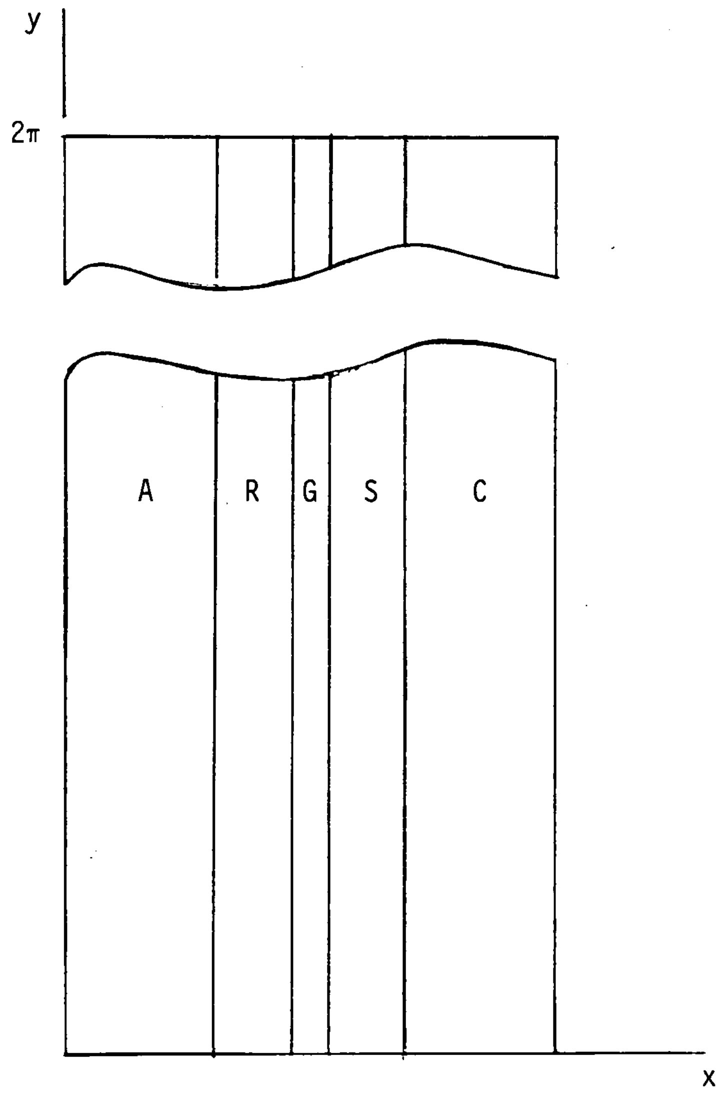

Figure 7. Computational Domain in
2D Inertial Rectangular
Cartesian Coordinates.

In three dimensional cartesian coordinates, the unsteady Euler equations may be written in conservation form as:

$$\frac{\partial \vec{G}}{\partial t} + \vec{\nabla} \cdot \bar{F} = 0 \qquad (1)$$

where:

$$\vec{G} = \begin{bmatrix} \rho \\ \rho u \\ \rho v \\ e \end{bmatrix}$$

$$\bar{F} = \begin{bmatrix} \rho u & \rho v \\ \rho u^2 + p & \rho uv \\ \rho uv & \rho v^2 + p \\ (e_v + p)u & (e_v + p)v \end{bmatrix}$$

and the pressure is obtained from:

$$p = (\gamma - 1)[e - \frac{\rho}{2}(u^2 + v^2)]. \qquad (2)$$

Equation (1) may be integrated over a small stationary volume $\forall$ to obtain:

$$\int_{\forall} \frac{\partial \vec{G}}{\partial t} d\forall + \int_{\forall} \vec{\nabla} \cdot \bar{F} d\forall = 0. \qquad (3)$$

An application of the mean value theorem to the first integral gives the result:

$$\forall \frac{\partial \vec{G}}{\partial t} + \int_{\forall} \vec{\nabla} \cdot \bar{F} \, d\forall = 0 \tag{4}$$

Now, upon defining $\hat{n}$ as the outward normal unit vector associated with s, the surface enclosing $\forall$, we have, by virtue of the divergence theorem:

$$\forall \frac{\partial \vec{G}}{\partial t} + \int_{s} \hat{n} \cdot \bar{F} \, ds = 0 \tag{5}$$

or,

$$\frac{\partial \vec{G}}{\partial t} = - \frac{1}{\forall} \int_{s} \hat{n} \cdot \bar{F} \, ds. \tag{6}$$

Here, the vector of conservation variables, $\vec{G}$, is associated with some point interior to the volume $\forall$ and is taken to be the center of $\forall$ for practical purposes.

The flux integral which comprises the right hand side of equation (6), may be approximated by summing the scalar products of the area vectors and the appropriately evaluated flux vectors.

The two step MacCormack algorithm, which is spatially and temporally second order accurate, is given by:

PREDICTOR:

$$\hat{G}^{N+1} = G^N - \frac{\omega \Delta t}{\forall} \left(\sum_k F_k \cdot S_k^+ + \sum_k F_k^- \cdot S_k^- \right) \tag{7}$$

CORRECTOR:

$$G^{N+1} = \frac{1}{2\omega} \hat{G}^{N+1} + \left(1 - \frac{1}{2\omega}\right) G^N - \frac{\Delta t}{\forall} \left(\sum_k \hat{F}_k^+ \cdot S_s^+ + \sum_k \hat{F}_k \cdot S_k^- \right) \tag{8}$$

where F_k is the flux vector approximated at the volume center, F_k^- is the flux vector approximated at the center point of the volume sharing the S_k^- face and F_k^+ corresponds in an analogous manner with S_k^+. The overbar is indicative of the predictor time level.

The parameter ω, appearing in equations (7) and (8) was introduced into the original ARO-1 code for stability considerations. In this investigation, ω was set equal to unity which has the effect of preserving the volume flux form of the MacCormack algorithm. The time step, Δt, was limited in magnitude by the familiar Courant-Friedrich-Lewy stability criterion. The maximum permissible time increment was computed as the minimum of

$$\Delta t = \frac{\forall}{|\vec{q} \cdot \vec{s}| + c\,|\vec{s}|} \tag{9}$$

over the entire mesh for each face of each volume. In this equation, c is the local sonic velocity and $\vec{q}$ is the velocity vector.

Compressor Blade Row Model

As previously stated, the unsteady Euler equations were integrated in the two duct-flow regions and in the rotor/stator gap. In two dimensions, this necessitated the solution of the equations governing continuity, axial and tangential momentum, and energy. Within the volume originally occupied by the rotor and stator, the effects of the presence of the rotor and stator blades were modeled by enforcing two algebraic constraint equations in lieu of two of the differential continuum equations. These constraint equations amount to a specification of the relative flow angle and, secondly, a specification of the losses associated with the passage of the flow through the blade row.

The equations to be solved within the blade volumes are:

$$\frac{\partial \rho}{\partial t} + \vec{\nabla} \cdot \rho\vec{V} = 0 \qquad \text{continuity} \tag{10}$$

$$\frac{\partial \rho e}{\partial t} + \vec{\nabla} \cdot \rho H\vec{V} = \dot{w} \qquad \text{energy} \tag{11}$$

$$\left\{\begin{array}{lll} s(\theta,t) & \text{Given from unsteady cascade loss model} & (12) \\ & & \\ \beta(\theta,t) & \text{Given from blade camberline angle plus} & (13) \\ & \text{unsteady cascade deviation angle} & \end{array}\right.$$

where H is the total enthalpy, defined by:

$$H = h + \frac{V^2}{2} + gz \tag{14}$$

and $\dot{w}$ is the work rate per unit volume being provided by the blade row. Integrating the energy equation over a small stationary volume gives, by the divergence and mean value theorems:

$$\forall \frac{\partial e_v}{\partial t} + \int_S H_v \vec{V} \cdot \vec{n} \, ds = \dot{W} \tag{15}$$

where $\dot{W}$ is the time rate of doing work.

The work term in equation (15) must be the same as that expended by the axial compressor in changing the tangential velocity of the fluid elements passing through the machine. This work may be quantified by integrating the tangential forces acting on the rotor, f_y, times the rotor tangential speed, ωr:

$$\dot{W} = \int_{\forall} r\omega f_y \, d\forall \tag{16}$$

or, as in the present case, for a constant radius and ω:

$$\dot{W} = r\omega \int_{\forall} f_y \, d\forall. \tag{17}$$

This integral may be evaluated by means of the tangential momentum equation:

$$\int_{\forall} f_y \, d\forall = \int_S p(\hat{j} \cdot \hat{n}) ds + \int_{\forall} \frac{\partial}{\partial t}(\rho v) d\forall + \int_S v\rho(\vec{V} \cdot \hat{n}) ds. \quad (18)$$

That is, multiplication of equation (18) by the linear rotor speed yields an expression for the work done on a given fluid element by the rotor:

$$\dot{W} = r\omega \{ \int_S p(\hat{j} \cdot \hat{n}) ds + \int_{\forall} \frac{\partial}{\partial t} (\rho v) d\forall + \int_S v\rho(\vec{V} \cdot \vec{n}) ds \}. \quad (19)$$

An application of the mean value theorem once again and subsequent substitution into (15) results in:

$$\forall \frac{\partial}{\partial t} e_V + \int_S H_V \vec{V} \cdot \hat{n} ds = r\omega \{ \int_S p(\hat{j} \cdot \hat{n}) ds + \frac{\partial}{\partial t} (\rho v) \forall + \int_S v\rho(\vec{V} \cdot \vec{n}) ds \}. \quad (20)$$

Defining a new variable E_2:

$$E_2 = e_V - r\omega\rho v \quad (21)$$

we have that:

$$\frac{\partial}{\partial t} E_2 = \frac{1}{\forall} \{ r\omega (\int_S p(\hat{j} \cdot \hat{n}) ds + \int_S v\rho(\vec{V} \cdot \hat{n}) ds) - \int_S H_V \vec{V} \cdot \hat{n} ds \}. \quad (22)$$

In terms of the scalar products of fluxes and areas in the ARO-1 code, equation (22) may be thought of in general terms as:

$$E_2^{N+1} = E_2^N - \frac{\Delta t}{\forall}\{F_5 - r\omega F_3\} \tag{23}$$

where F_5, the energy flux integral, is given by:

$$F_5 = \int_S H_v \vec{V} \cdot \hat{n} ds \tag{24}$$

and F_3 is the tangential momentum flux integral:

$$F_3 = \int_S (p(\hat{j} \cdot \hat{n}) + v\rho(\vec{V} \cdot \hat{n}))ds. \tag{25}$$

Equation (22) was integrated in time via the MacCormack predictor-corrector algorithm. The quantity E_2 was then applied in the following manner: Since,

$$e_v = \rho\{C_v T + \frac{q}{2}\} \tag{26}$$

and $$q = \frac{1}{2}(u^2 + v^2) \tag{27}$$

it then follows that

$$e_v = \rho C_v T + \frac{\rho}{2}(u^2 + v^2). \tag{28}$$

Also, since

$$u = V \cos \theta \tag{29}$$

and

$$v = V \sin \theta \tag{30}$$

then

$$e_v = \rho C_v T + \frac{\rho V^2}{2} . \tag{31}$$

And, combining equations (21) and (31) there follows:

$$E_2 = \frac{p}{\gamma - 1} + \frac{1}{2}\rho V^2 - \frac{\rho r \omega}{g_c} V \sin \theta . \tag{32}$$

Equation (32) constitutes one of the two algebraic constraint equations that replace two of the continuum equations in the compressor blade rows. The second equation follows directly from the constraint of the relative flow angle. This angle is to be taken as the angle of the mean camberline plus a deviation. Referring to the velocity triangle of Figure 8, the absolute flow velocity $\vec{V}$ is related to the relative flow velocity $\vec{w}$ and the rotor speed $\vec{ws}$ by:

$$\vec{V} = \vec{W} + \vec{ws} \tag{33}$$

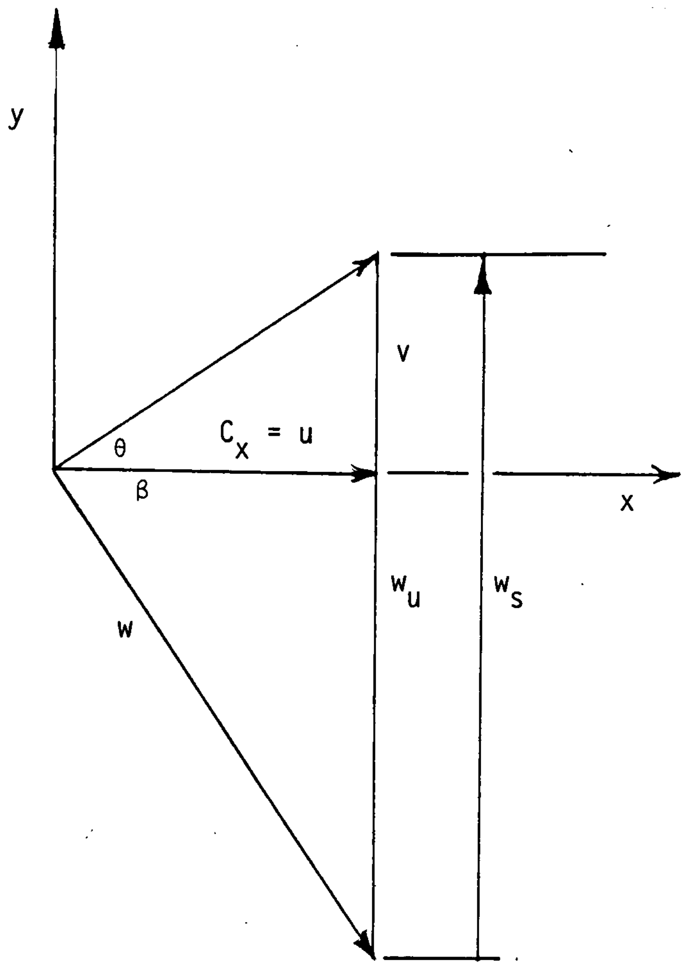

Figure 8. Velocity Triangle Nomenclature.

Analogously, in terms of tangential components:

$$\vec{V} = \vec{W}_u + \vec{W}s. \tag{34}$$

Referring to Figure 8, some simple trigonometry may be employed to express this as:

$$\sin\theta - \frac{Ws}{V} - \cos\theta \tan\beta = 0. \tag{35}$$

Equations (32) and (35) constitute two equations in the unknowns V and θ that are solved for iteratively by Newton's method based on the updated values of E_2 and ρ. Since the losses and the relative flow angle are specified by the unsteady cascade models, all of the thermodynamic variables at each compressor node may be updated at the new time level.

CHAPTER III

BOUNDARY CONDITIONS

Axial Characteristic Boundary Condition

An analysis of the boundary conditions pertinent to this problem is perhaps best facilitated by firstly discussing those boundary conditions associated with a one dimensional flow and subsequently expanding the discussion to two dimensions.

By writing the system of equations given by (1) in a single spatial dimension we have that:

$$\frac{\partial \vec{G}}{\partial t} + \frac{\partial \vec{F}}{\partial x} = 0. \tag{36}$$

It is rather fortuitous that the vector $\vec{F}$ is a homogeneous function of the axial component of flow velocity $\vec{u}$. This allows one to write:

$$\frac{\partial \vec{F}}{\partial x} = \frac{\partial \vec{F}}{\partial \vec{u}} \frac{\partial \vec{u}}{\partial x} \tag{37}$$

where $\frac{\partial \vec{F}}{\partial \vec{u}}$ is known as the Jacobian Matrix of this system of equations. As shown by Reddy and Tsui [12], this Jacobian matrix has exactly three real-valued and distinct eigenvalues: u, u+c, u-c. Since the eigenvalues of this system of partial differential equations are real and distinct, this system of governing equations is by definition hyperbolic in type. The theory of partial differential equations dictates that the necessary and sufficient number of boundary conditions to be imposed on a given inflow boundary is equal to the number of positive eigenvalues extant at that boundary. Thus, for a subsonic inlet flow we require two specifications corresponding to the eigenvalues u and u+c. These eigenvalues are associated with the right-running characteristics shown in Figure 9 while the left-running inlet characteristic corresponds to the u-c eigenvalue.

The theory of partial differential equations analogously dictates that the necessary and sufficient number of exit flow boundary specifications is equal to the number of negative eigenvalues of the Jacobian Matrix at the exit. Thus for a one dimensional subsonic flow exactly one exit boundary condition is required.

In a one dimensional calculation, the three conservation equations of mass, momentum, and energy conservation must be satisfied. Thus, there are three boundary conditions that must be specified at both the inlet and the exit, though only two and one respectively may be specified arbitrarily. Thus, there remains one relationship at the inlet and two relationships at the exit to be applied in order to ensure a well-posed problem. Since the equation system is hyperbolic in type, the method of characteristics is a preferred technique in obtaining these relationships, largely because it gives accurate and reliable results. As derived in [12] there exists a compatibility equation along each of the three characteristic directions:

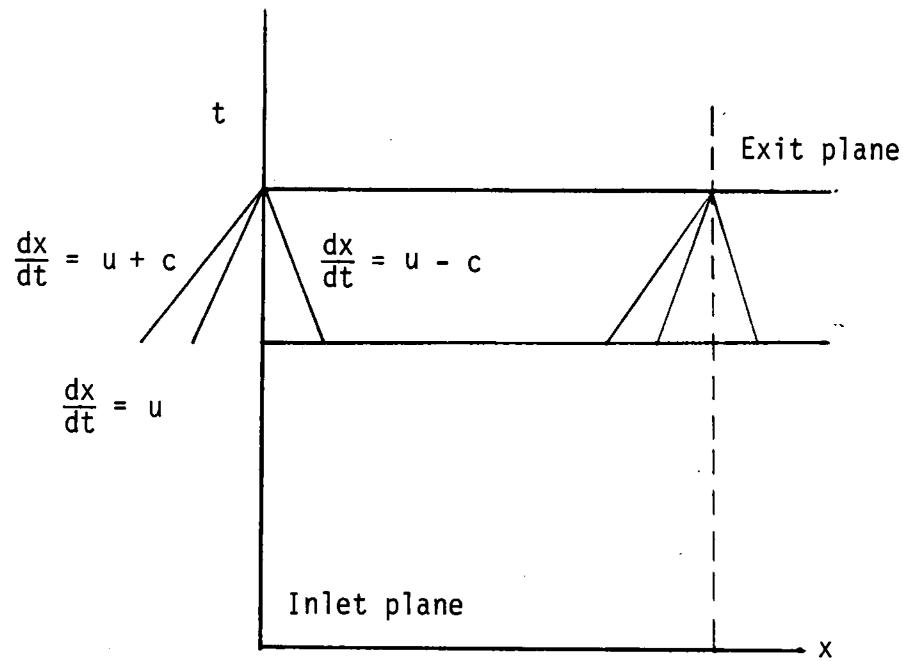

Figure 9. One Dimensional Inlet and Exit Characteristic Directions.

$$c^2 \frac{d\rho}{dt} - \frac{dp}{dt} = \text{zero} \quad \text{along} \quad \frac{dx}{dt} = u \tag{38}$$

$$\rho c \frac{du}{dt} + \frac{dp}{dt} = \text{zero} \quad \text{along} \quad \frac{dx}{dt} = u + c \tag{39}$$

$$-\rho c \frac{du}{dt} + \frac{dp}{dt} = \text{zero} \quad \text{along} \quad \frac{dx}{dt} = u - c \tag{40}$$

It is useful to note that these equations are equivalent to the original set of governing equations and could therefore be used to advance the solution at all interior points of the domain in addition to the boundary nodes.

In the two dimensional flow of present interest, disturbances propagate not along characteristic lines but rather along a conoidal characteristic surface. Erdos, Alzner and McNally [13] approximated this true characteristic form by formulating the governing system of equations in a reference plane coordinate system which reduces the dimensions of the characteristic plane to a more tractable form. Erdos et al. envisioned this reference plane as being normal to both the x-y plane (time=constant) and also to the inlet station (x=constant). In addition, if this reference plane is allowed to translate in the y direction at the same speed as the tangential component of the flow velocity v we have the representation shown in Figure 10.

The compatibility relations for constant x plane reference characteristics may be derived in a manner analogous to that found in reference [12] as:

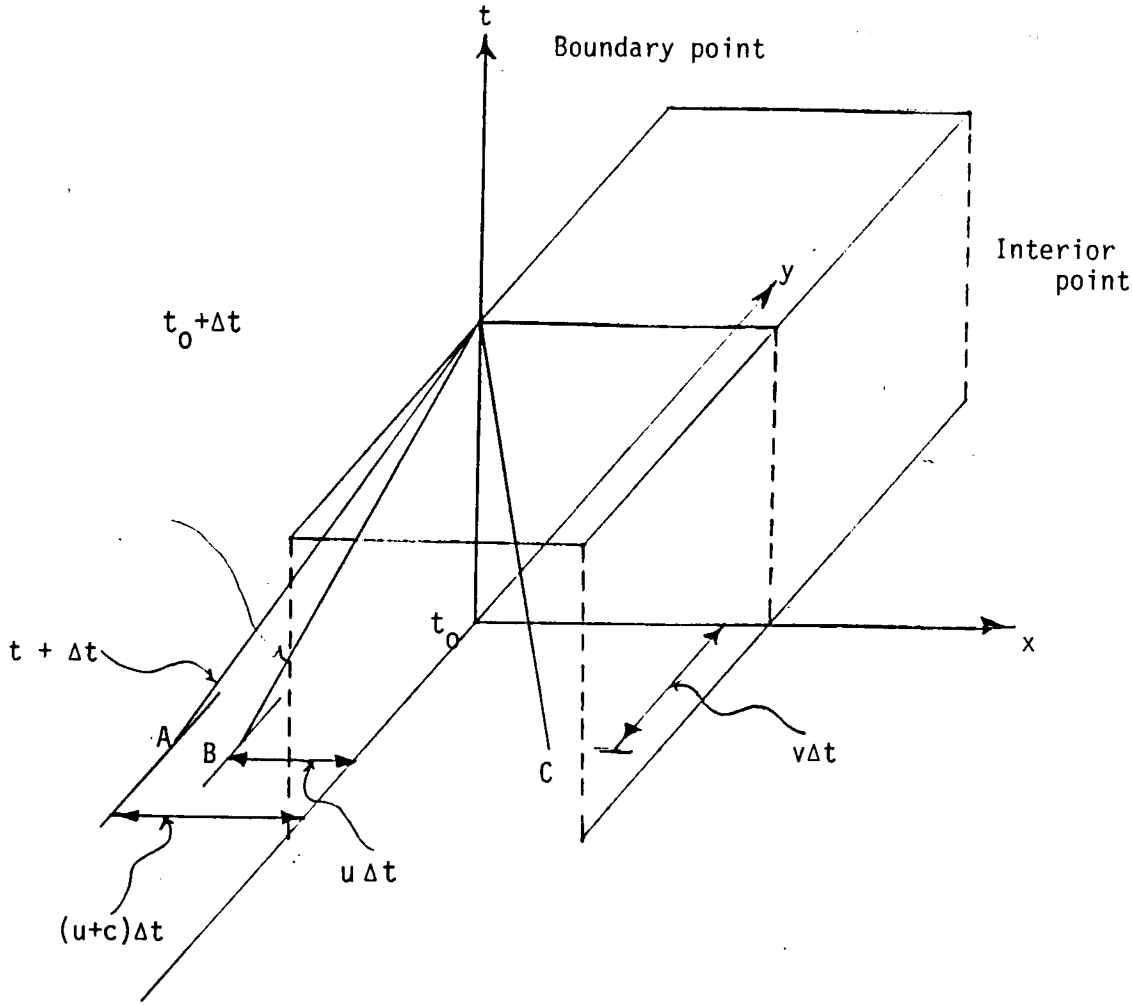

Figure 10. Characteristic Lines and Grid Points for Use in Reference Plane Boundary Conditions.

$$\frac{Du}{Dt} = \frac{1}{2c}\frac{Dp}{Dt} - v\frac{\partial \rho}{\partial y} + \frac{v}{c^2}\frac{\partial p}{\partial y} \tag{41}$$

$$\frac{Dv}{Dt} = -v\frac{\partial v}{\partial y} - \frac{1}{\rho}\frac{\partial p}{\partial y} \tag{42}$$

$$\frac{Du}{Dt} = \frac{-1}{\rho c}\frac{Dp}{Dt} - v\frac{\partial u}{\partial y} - c\frac{\partial v}{\partial y} - \frac{v}{\rho c}\frac{\partial p}{\partial y} \tag{43}$$

$$\frac{Du}{Dt} = \frac{1}{\rho c}\frac{Dp}{Dt} - v\frac{\partial u}{\partial y} + c\frac{\partial v}{\partial y} + \frac{v}{\rho c}\frac{\partial p}{\partial y} \tag{44}$$

For subsonic inflow, equation (44) must be employed to specify u. The complete set of eigenvectors pertaining to this two dimensional flow can be shown to be u, v, u+c, u-c, v+c, and v-c. Since the tangential component may be positive or negative, there are three positive eigenvectors at the inlet and therefore three quantities may be arbitrarily specified there. In the present study these quantities were chosen to be total pressure, total temperature and the absolute flow angle.

Corresponding to the single left-running characteristic at the exit plane, exactly one boundary specification need be arbitrarily assigned there. In this study, the static pressure was specified as a function of time in order to control the back pressure experienced by the compressor. Additionally a zero gradient specification was imposed on all other variables at the exit plane.

Circumferential Periodic Boundary Condition

The boundary conditions in the circumferential direction were specified to be periodic in nature. This was accomplished by a simple equation process as depicted in Figure 11.

Radial Mirror Boundary Condition

Mirror conditions were used at the surface boundaries. This consists of setting pressure, density and energy at the phantom boundary points equal to the adjacent interior values. Additionally, the velocity vector is mirrored using:

$$\vec{q}_{bc} = \vec{q}_{in} - 2 \cdot \left\{ \frac{\vec{S} \cdot \vec{q}_{in}}{\vec{S} \cdot \vec{S}} \right\} \vec{S} \tag{45}$$

where $\vec{q}_{bc}$ is the velocity vector at the phantom point adjacent to $\vec{q}_{in}$ and S is the boundary area vector.

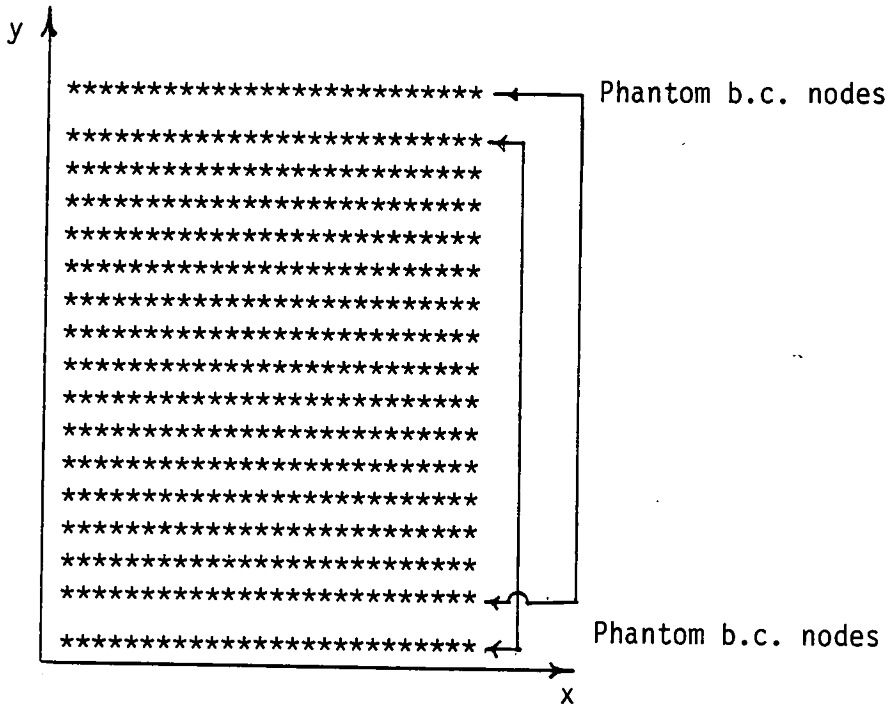

Figure 11. Periodic Tangential Boundary Conditions.

CHAPTER IV

THE UNSTEADY CASCADE LOSS MODEL

It is assumed that the total loss experienced by each fluid particle upon exit from the cascade is determined by the instantaneous conditions (i.e., incidence angle and relative Mach number) it encountered when it entered the cascade inlet (i.e., at the inlet at a previous time). Furthermore, we assume that this loss accumulates in a specified fashion--we assume linearly for lack of a better guess--from the cascade inlet to the exit.

This loss may be mathematically represented by:

$$\Delta S(\theta,\Delta t) = \Delta S(i(\theta-\Delta\theta,t-\Delta t),\ M(\theta-\Delta\theta,t-\Delta t)) \tag{46}$$

where i and M are the inflow incidence angle and relative Mach number respectively; $\theta-\Delta\theta$ is the tangential location of the particle when it is located at the inlet; and $t-\Delta t$ is the time at which the particle is present at the inlet.

Since this loss is determined uniquely for each fluid particle by its inlet value,

$$\frac{D}{Dt}\Delta S = 0. \tag{47}$$

In addition, the initial value of the entropy, S_i, associated with the particle upon entry to the cascade is required. This quantity is also invariant as the particle traverses the cascade, enabling one to write:

$$\frac{D}{Dt} S_i = 0. \tag{48}$$

Let ϕ represent either ΔS or S_i. Then, by definition,

$$\frac{D\phi}{Dt} = \frac{\partial \phi}{\partial t} + \vec{V} \cdot \vec{\nabla}\phi = 0 \tag{49}$$

or

$$\frac{\partial \phi}{\partial t} + u \frac{\partial \phi}{\partial x} + v \frac{\partial \phi}{\partial y} = 0. \tag{50}$$

The terms of equation (50) are discretized at each grid node (I,J) as follows:

$$\frac{\partial \phi}{\partial t} = \left. \frac{\phi(t+\Delta t) - \phi(t)}{\Delta t} \right|_{I,J} \tag{51}$$

(where Δt is the time step)

$$\frac{\partial \phi}{\partial x} = \left. \frac{\phi(I,J) - \phi(I-1,J)}{\Delta x} \right|_{t} \tag{52}$$

$$\frac{\partial\phi}{\partial y} = \left.\frac{\phi(I,J) - \phi(I,J-1)}{\Delta y}\right|_t \quad v \geq 0$$

$$\frac{\partial\phi}{\partial y} = \left.\frac{\phi(I,J+1) - \phi(I,J)}{\Delta y}\right|_t \quad v < 0 \tag{53}$$

where the upwind differences are employed to reflect the convective nature of the equation. Then, from equation (50),

$$\phi(t+\Delta t)|_{I,J} = \phi(t)|_{I,J} - \Delta t\left(u(t)\,\frac{\Delta\phi}{\Delta x} + v(t)\,\frac{\Delta\phi}{\Delta y}\right). \tag{54}$$

With ΔS and S_i integrated from t to $(t+\Delta t)$ by equation (54), the particle entropy is updated from:

$$S_{I,J} = S_{i_{I,J}} + \frac{x}{c}\,\Delta S_{I,J} \tag{55}$$

where c is the axial chord.

The governing relationship for the entering entropy, S_i, may be attained by combining the first and second laws of thermodynamics to obtain:

$$Tds = dh - \frac{dp}{\rho}. \tag{56}$$

By applying the perfect gas law and integrating:

$$S_2 - S_1 = \int_1^2 C_p \frac{dT}{T} - \int_1^2 R \frac{dP}{P} . \tag{57}$$

Assuming constant specific heats, this becomes

$$S_2 - S_1 = C_p \ln \frac{T_2}{T_1} - R \ln \frac{P_2}{P_1} \tag{58}$$

which can be equivalently stated as

$$S_1 = C_p \ln \frac{\rho_{ref}}{\rho} + C_v \ln \frac{p}{p_{ref}} . \tag{59}$$

Cascade losses are usually quantified in terms of a loss coefficient rather than in terms of changes in entropy. The definition of $\bar{\omega}$ gives:

$$\bar{\omega} = \frac{P_{ti}-P_t}{P_{ti}-P_i} \tag{60}$$

where the subscript i refers to inlet conditions and all quantities are referred to a coordinate system fixed to the blade. With this latter consideration one may write:

$$\frac{P_t}{P_{ti}} = e^{-\Delta S/R} \tag{61}$$

such that

$$\Delta S \;=\; -R \ln\{1 - \overline{\omega}(1 - P_i/P_{ti})\}. \qquad (62)$$

The loss coefficient $\overline{\omega}$, is an empirical quantity that is specified as a function of incidence angle and Mach number. In this initial investigation, the Mach number dependence was neglected and ω was specified according to Figure 12.

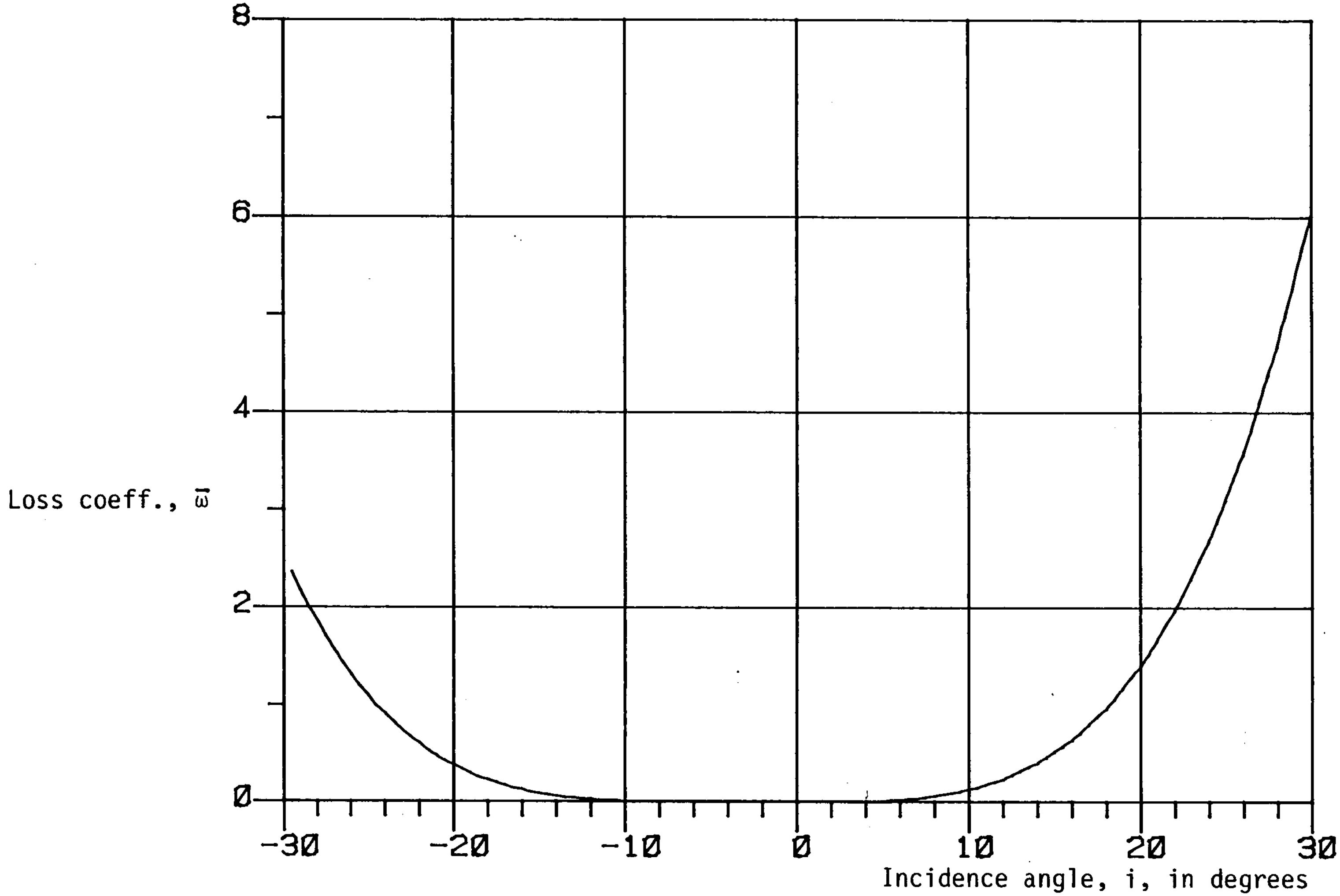

Figure 12. Specification of Loss Coefficient, $\bar{\omega}$, versus Incidence.

CHAPTER V

THE UNSTEADY CASCADE DEVIATION MODEL

The deviation angle δ is defined as the difference between the relative flow angle and the blade mean camber line angle. That is,

$$\delta = \angle_{rf} - \angle_{m}. \tag{63}$$

The rationale of the unsteady deviation model closely follows that of the unsteady loss model. An exception is that no initial deviation is attributed to the flow, i.e., at the rotor and stator inlets, δ is zero. Equations (49) through (53) apply and $\Delta\delta$ (the eventual deviation) is updated via equation (54). Finally, δ is spatially accounted for by:

$$\delta_{I,J} = \frac{x}{c}\,\Delta\delta_{I,J}. \tag{64}$$

The deviation angle, like the loss coefficient, is an empirical quantity that varies as a function of incidence and Mach number. The dependence of $\Delta\delta$ on Mach number was herein neglected, with $\Delta\delta$ specified according to Figure 13. With the deviation angle known, the relative flow angle in the rotor and stator is updated according to:

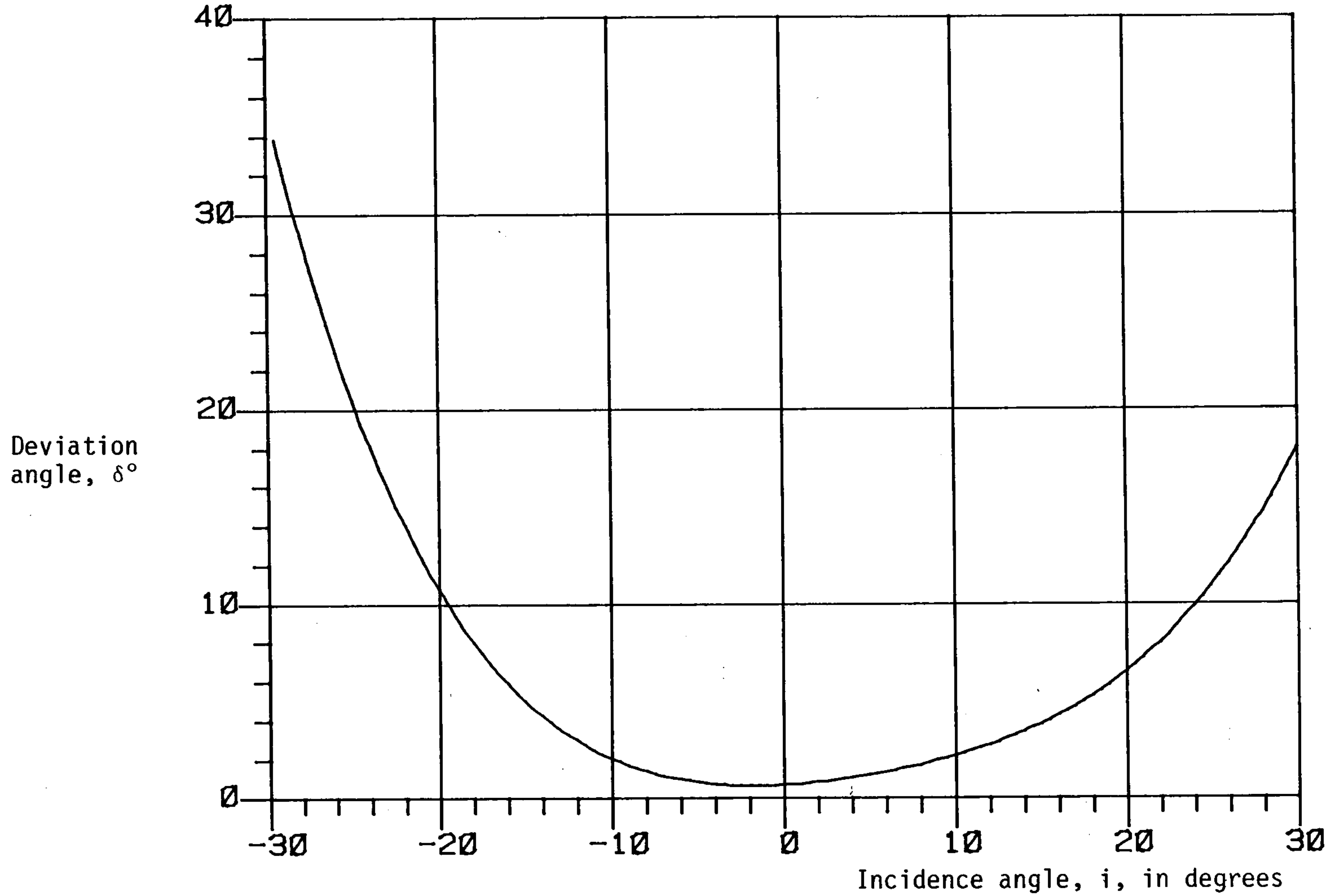

Figure 13. Specification of Deviation Angle, δ, versus Incidence.

$$\beta_r = \angle_m - \frac{x}{c}\,\Delta\delta_r \tag{65}$$

in the rotor and

$$\beta_s = \angle_m - \frac{x}{c}\,\Delta\delta_s \tag{66}$$

in the stator. The method of implementing these unsteady loss and deviation angle models possesses an important advantage in that they circumvent the necessity to store the temporal and spatial history of each flow particle and its associated loss and deviation characteristics.

CHAPTER VI

RESULTS AND CONCLUSIONS

A mathematical and numerical model was developed in order to simulate the operation of a single stage axial compressor. This model was evaluated firstly by implementing a flat blade rotor and stator as depicted in Figure 14. The blade angles of the rotor and stator were initially defined so as to generate zero incidence (and, therefore, zero pressure rise) for the purpose of checking the accuracy in coding of the model. Operation of the code in this initial phase resulted in stable operation at the nominal operating point (NOP). As the next phase in the code validation, the exit static pressure was ramped at 50 psi/sec in order to place the rotor and stator at incidence and, therefore, generate a pressure rise across the compressor. At this point, a distinct spatial oscillation in all the solution quantities became apparent. The source of this oscillation was subsequently traced to the manner in which the algebraic constraint equations were blended with the Euler continuum equations at the leading edge of the rotor and of the stator. This problem was corrected by incorporating a set of unsteady source terms, as discussed in the Appendix.

With the flat blade model operating properly at incidence, a more realistic set of blading angles was calculated by assuming an

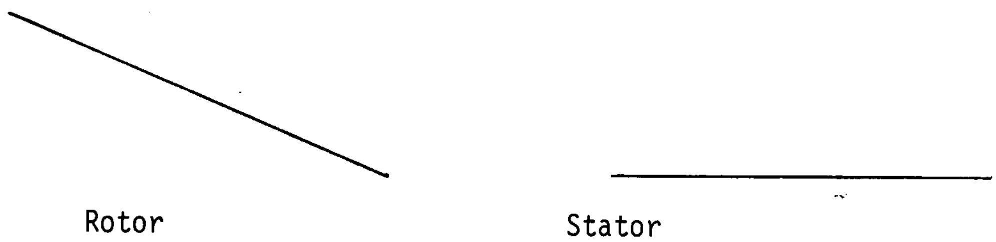

Figure 14. Flat Blade Rotor and Stator.

isentropic operating point and a desired pressure ratio. As depicted by Figure 15, this resulted in a discretely-curved blade row which inputs work by turning in addition to incidence.

The nominal operating point of the compressor model at this stage of development is as depicted in Figure 16. The correct isentropic operation of the model was verified at this time by switching off the loss and deviation models and ramping the exit pressure as previously.

The compressor characteristic of Figure 16 was traced from the NOP by elevating the exit static pressure in step increases and then marching in time at each pressure level to reach an asymptotic state. Upon further backpressuring past the maximum pressure coefficient the compressor developed a surge-like behavior depicted by the positive slope portion of the characteristic. These points were not fully converged but rather "transient" points obtained as the model proceeded to divergence.

At this stage in the code validation, it was thought that the surge-like behavior was due to unrealistically large values of the specified loss coefficient and deviation angle. Thus, limiting values were placed on these specifications and the above characteristic-tracing process was repeated. In the resulting characteristic shown in Figure 17, the point of maximum loss and deviation angle is apparent. Judging by the behavior of the characteristic at low flow, this was obviously not the correct approach.

Figure 15. Discretely-Curved Rotor and Stator.

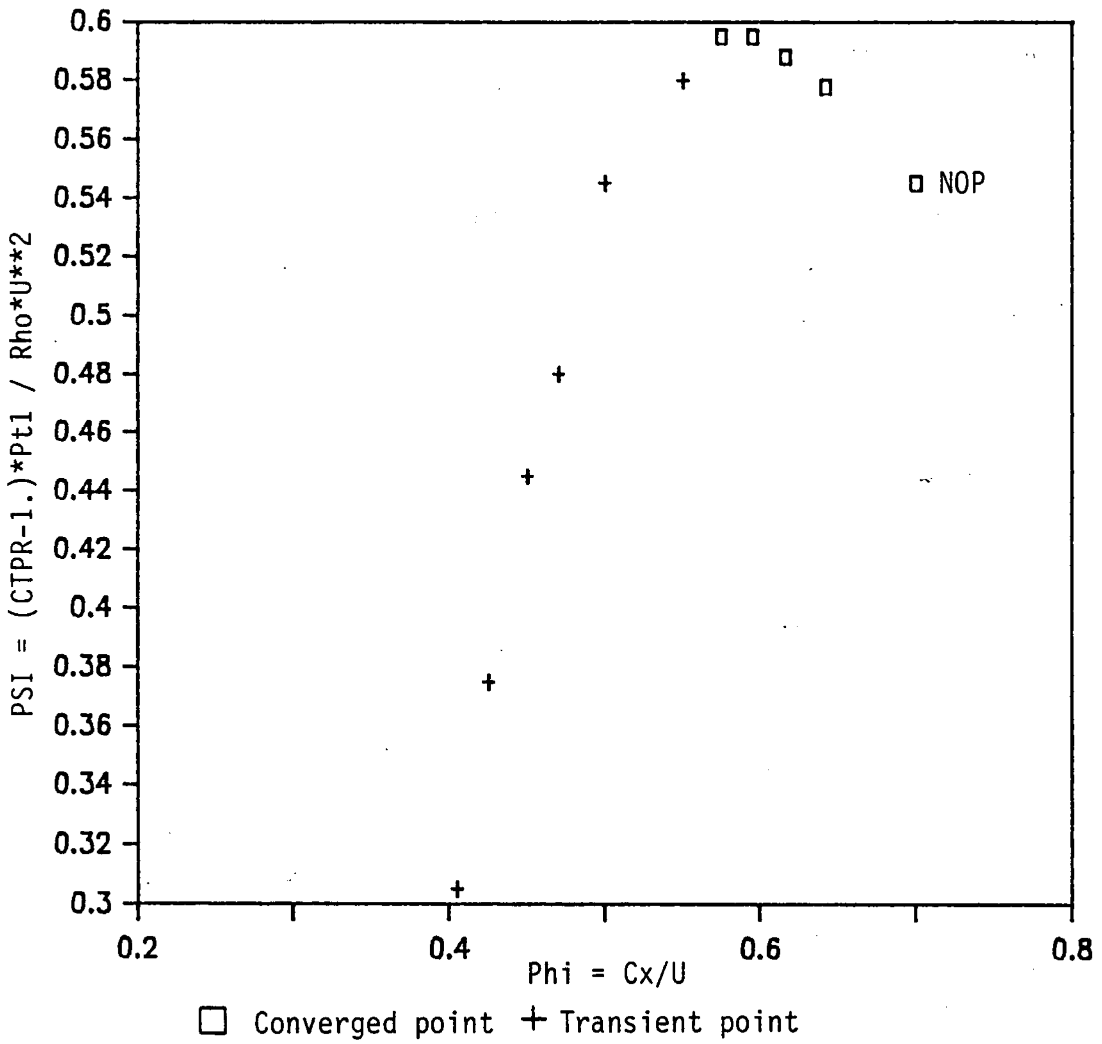

Figure 16. Computed Single Stage Compressor Characteristic.

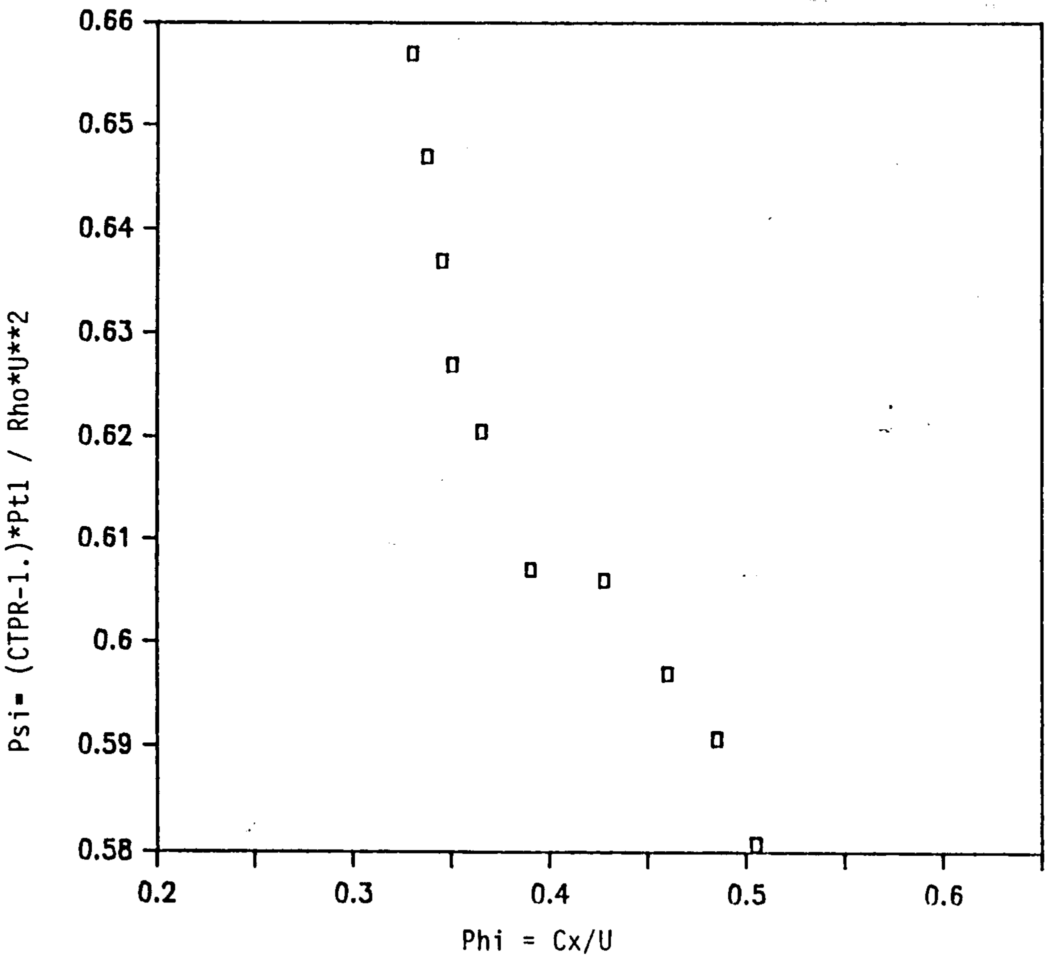

Figure 17. Computed Single Stage Compressor Characteristic with Maximum-Limited Loss and Deviation Specifications.

In the above attempts to develop a stable rotating stall pattern, it was assumed that existing random numerical fluctuations would be sufficient to instigate the phenomenon provided the compressor was sufficiently close to the neutral stability point (the point where the characteristic's slope is zero). This was apparently not the case. Therefore, a transient circumferential defect in inlet total pressure was imposed over approximately thirty percent of the compressor annulus in an attempt to instigate a rotating pattern. The results of this total pressure perturbation were found to depend on both the magnitude of the pressure defect and also the location of the operating point on the characteristic at which the defect was imposed. (This operating point was varied by maintaining the exit static pressure constant in time at several different levels.) That is, a defect of 1, 2, and 1 percent of the inlet total pressure imposed over three nodes respectively and applied on the negative slope portion of the characteristic resulted in a rapid return to the pre-perturbed state. A larger perturbation of 5, 10, and 5 percent applied at the same operating point caused the model to rapidly diverge. A temporal evolution of the conservation variable rho*u enroute to divergence is shown in Figure 18.

The neutral stability point was similarly perturbed using these two levels of total pressure defect. Imposition of the higher level of perturbation predictably caused the method to proceed to divergence. The more mild pressure defect caused the method to diverge much more slowly. Moreover, the distortion was observed to expand circumferentially in both directions away from the original location.

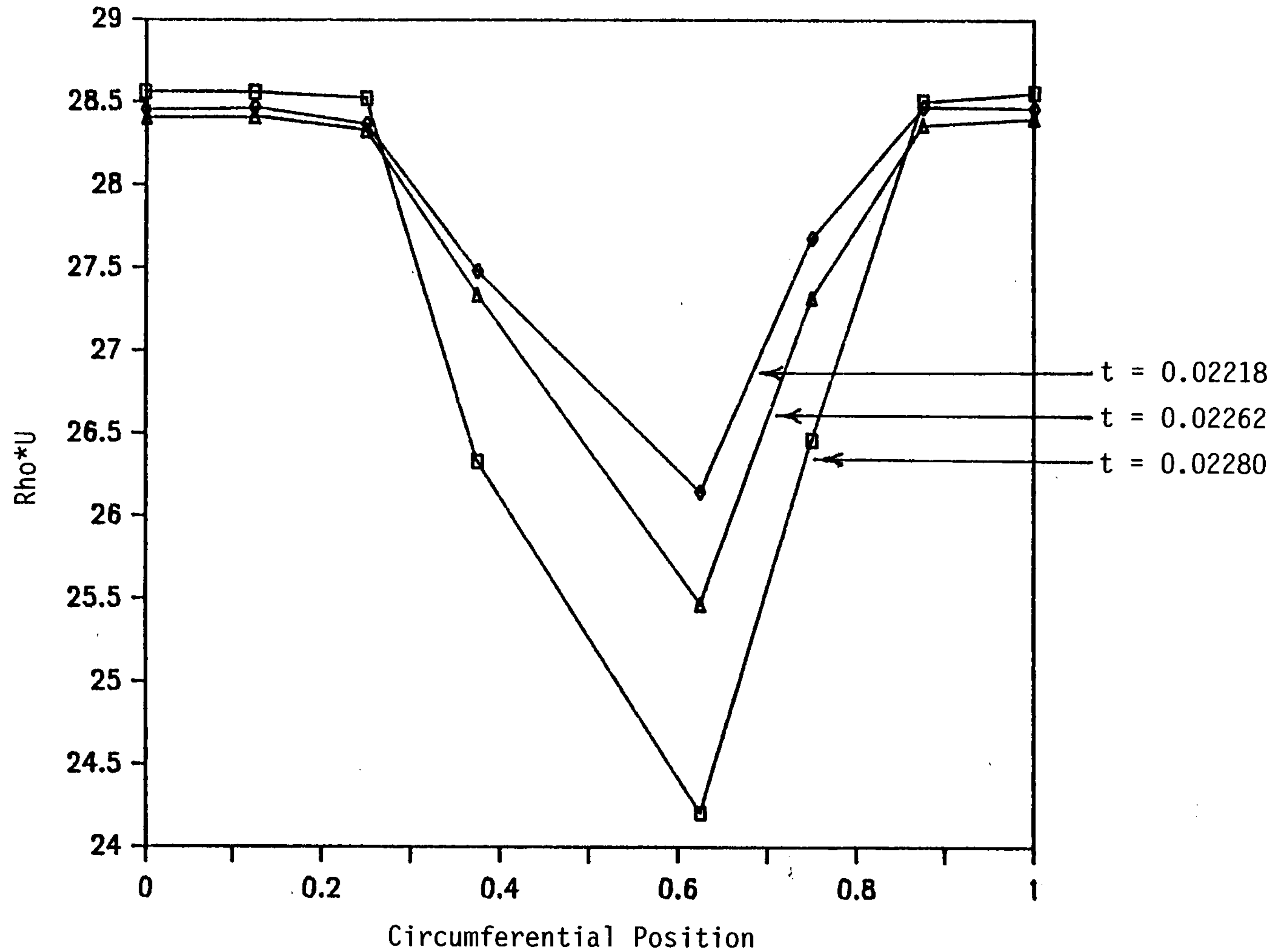

Figure 18. Temporal Evolution of Circumferential Distortion at Compressor Inlet.

It is emphasized that all of these perturbations were transient in nature, the dwell time being that necessary for the disturbance to travel from the duct inlet to the rotor inlet.

A careful consideration of the acquired results has evoked a large measure of confidence in the basic validity of the solution method. However, the lack of an appropriate throttle characteristic seems to have prevented the present method from operating stably at the neutral stability point.

Enroute to elucidating this idea, consider Figure 19, which depicts the performance map (flow coefficient versus pressure coefficient) of several pumps and fans. A single such machine may exhibit a variety of performance characteristics as a function of rotational speed as shown in Figure 20. Further, the pumping device almost invariably operates in some duct system whose characteristic would be similar to that of curve 1 of Figure 21. The steepness of this basic characteristic may be attenuated by the addition of a bleed or a subsystem (e.g., a second stage or a second pump) (curve 3) or it may be made steeper by the addition of a throttling device (curve 2).

Two different pumping systems operating in the same duct system are contrasted in Figure 22 which is after Emmons [4]. For both compressors, the nominal operating point, 0, is that at which the pressure rise of the pumping device just matches the pressure drop attributed to the duct system. This operating point is stable if the pump has a negative slope characteristic, since all duct system characteristics are positive. This may be made apparent by considering

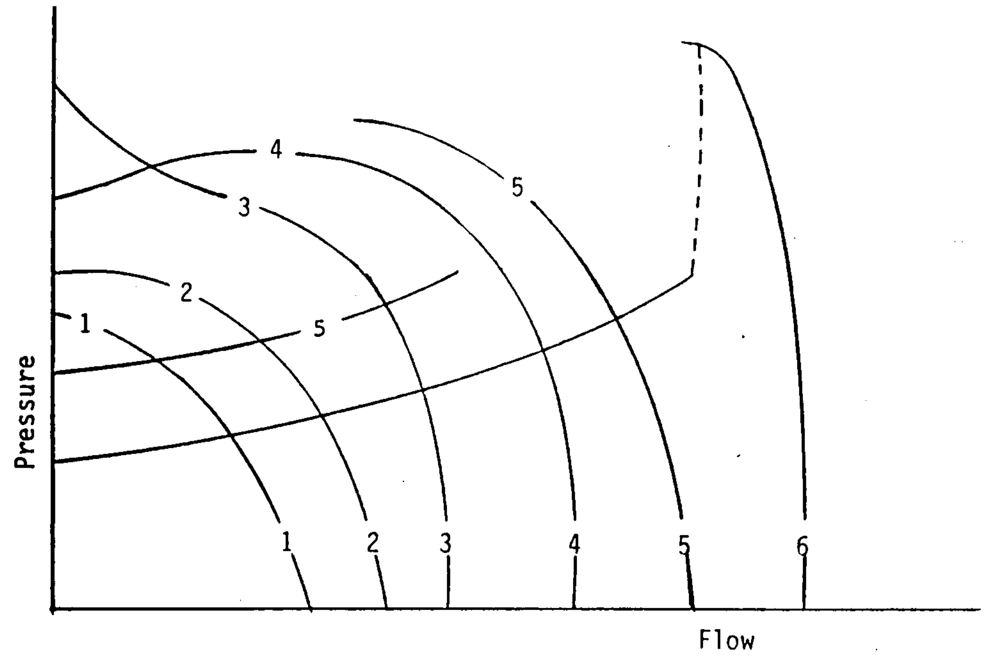

Figure 19. Characteristics of Various Pumping Systems.

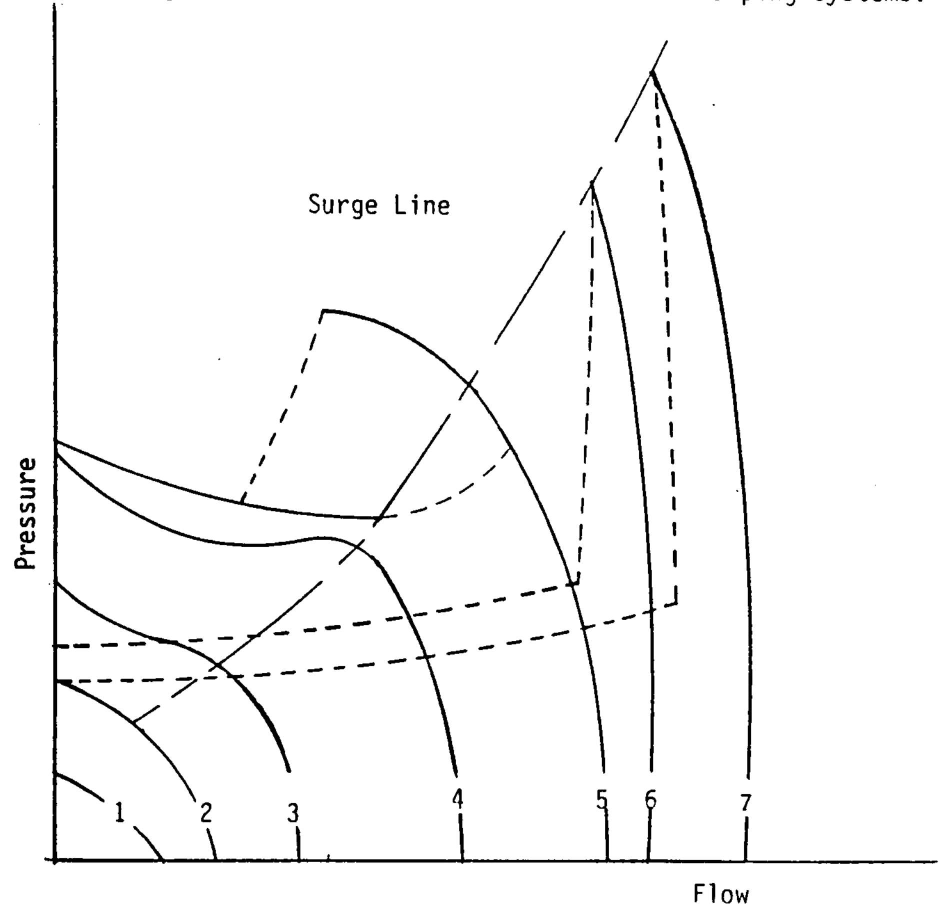

Figure 20. Compressor Characteristics Over a Wide Range in Speed.

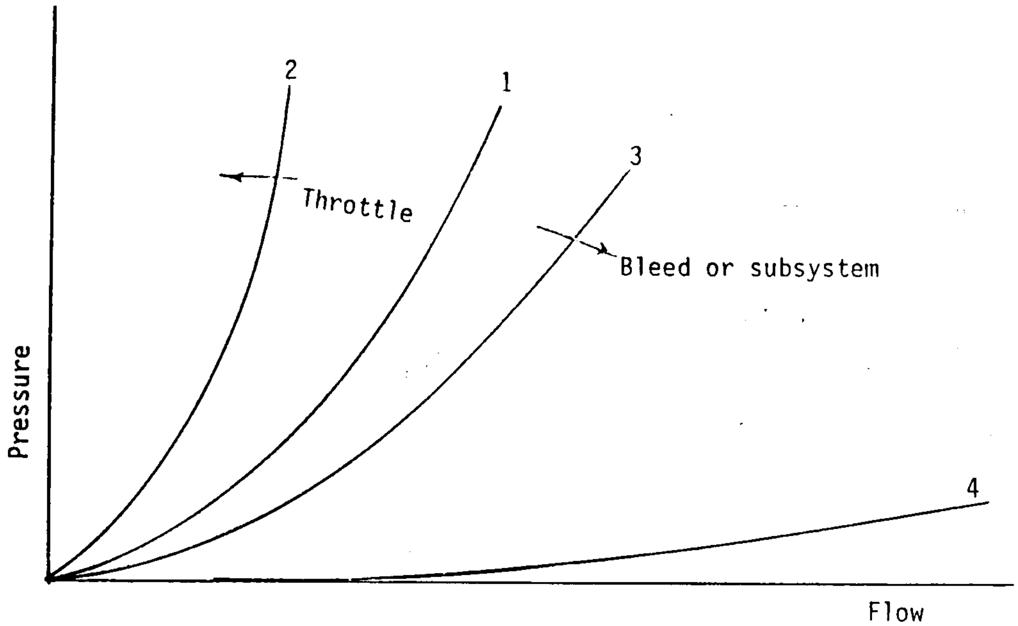

Figure 21. Typical System Pressure Requirements.

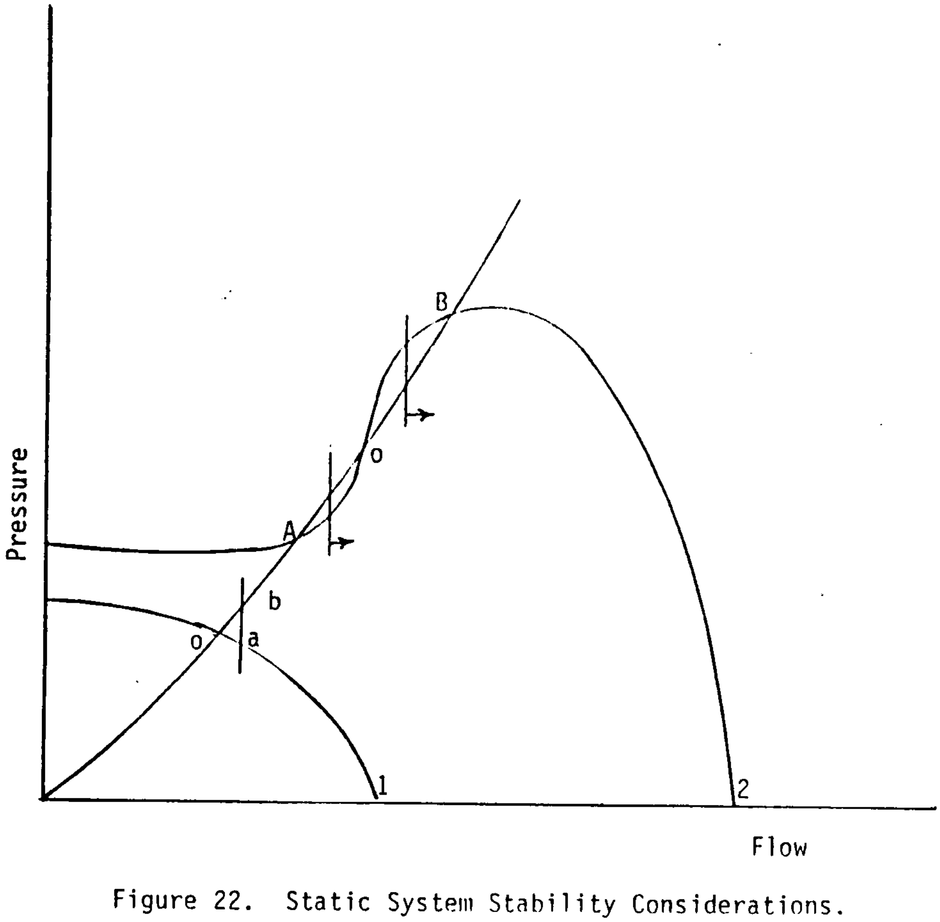

Figure 22. Static System Stability Considerations.

a perturbation of the operating point of compressor 1 of Figure 22. Assuming a sudden increase in flowrate, the pressure loss of the duct system (b) is greater than that pressure rise developed in the pump (a). Fluid inertia supplies this difference in pressure. Hence, the fluid decelerates and the stable operating point 0 is re-established.

A similar perturbation to operating point 0 of pump 2 has a quite dissimilar result due to the positive slope of the pump characteristic. Again, assuming a sudden increase in flow rate, the pump generates a pressure difference in excess of the system loss which is then expended in accelerating the fluid. This results in a short interval of unsteady operation culminating in the establishment of a stable operating point at B. Conversely, a sudden decrease in flowrate precedes the establishment of the stable operating point A. The obvious conclusion is that some system pump combinations may possess multiple stable operating points.

In the present investigation, no explicit system characteristic was imposed. The result was not the absence of a system characteristic but rather an effective characteristic such as those depicted in Figure 23. These two system characteristics correspond to two different levels of (constant) exit static pressure. By the above discussion, operating point A of Figure 23 is stable. This point corresponds to the aforementioned small total pressure perturbation experiments wherein the flow returned to its pre-perturbed state. Larger perturbations caused the operating point to move to point C where the distortion amplified--culminating in a failure of the method.

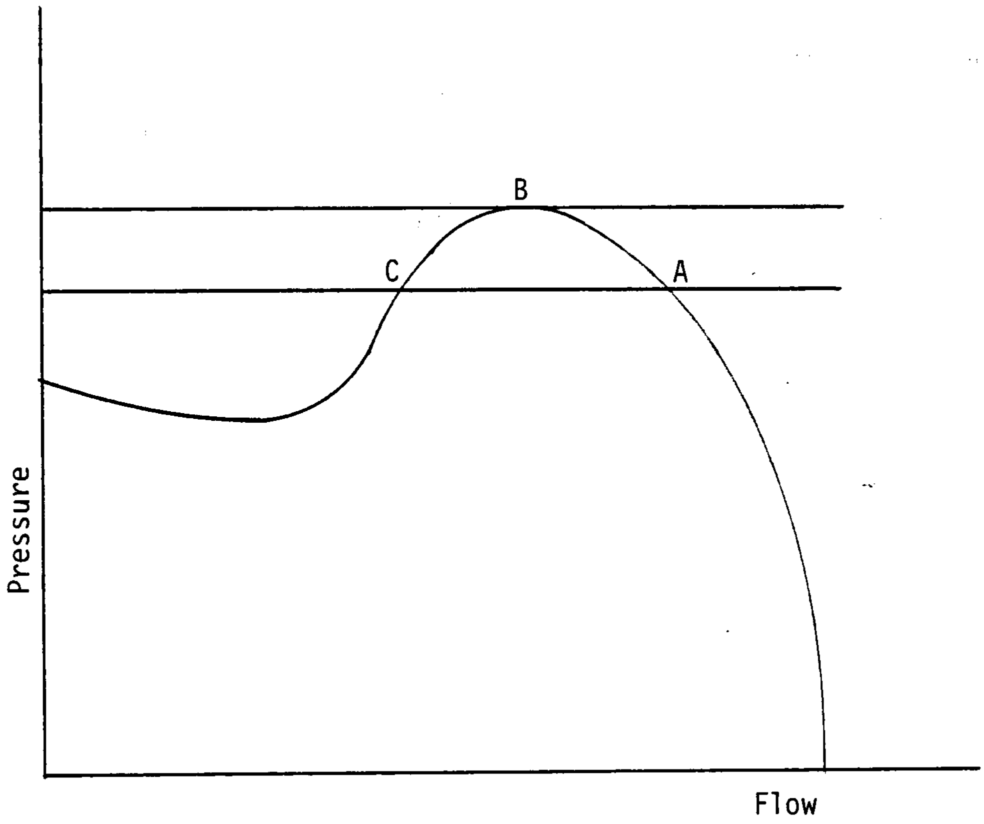

Figure 23. Implicit Throttle Characteristics.

Perturbations applied at the neutral stability point B similarly drove the operating point in the direction of point C.

Apparently what is required is a positive-slope system characteristic intersecting the neutral stability point. This would allow the method to operate stably on the part of the characteristic associated with partial stall.

CHAPTER VII

RECOMMENDATIONS

It appears likely that the lack of an appropriate throttle characteristic prevented the present method from operating stably on the part of the characteristic associated with partial stall. With this inclusion the method has good potential in numerically producing at least a qualitatively accurate rotating stall. Once this goal is attained, the method should be checked for grid independence, as this proved to be a drawback to a previous numerical study by Pandolfi [11]. A next step would be to analyze an existing compressor for which data are available to check for quantitative accuracy in the stall emulation. This step should also include loss and deviation characteristics pertaining to the stalled operating condition and dependent upon Mach number as well as incidence.

LIST OF REFERENCES

LIST OF REFERENCES

1. Jacocks, J. L., and Kneile, K. R. "Computation of Three Dimensional Time-Dependent Flow Using the Euler Equations," AEDC-TR-80-49, 1980.

2. MacCormack, R. W. "The Effect of Viscosity in Hypervelocity Impact Cratering," AIAA Paper No. 69-354, 1969.

3. Cumpsty, N. A., and Greitzer, E. M. "A Simple Model for Compressor Stall Cell Propagation," ASME Paper No. 81-GT-73, 1973.

4. Emmons, H. W., Pearson, C. E., and Grant, H. P. "Compressor Surge and Stall Propagation," Transactions of the American Society of Mechanical Engineers, May, 1955, pp. 455-469.

5. Day, I. J., Greitzer, E. M., and Cumpsty, N. A. "Prediction of Compressor Performance in Rotating Stall," ASME Paper No. 77-GT-10, 1977.

6. Day, I. J., and Cumpsty, N. A. "The Measurement and Interpretation of Flow Within Rotating Stall Cells in Axial Compressors," Journal of Mechanical Engineering Science, Vol. 20, No. 2, 1978.

7. Lakhwani, C., and Marsh, H. "Rotating Stall in an Isolated Rotor Row and a Single Stage Compressor," Instn. Mech. Engrs., Paper No. C58/73, 1973.

8. Sexton, M. R., and O'Brien, W. F., Jr. "A Model for Dynamic Loss Response in Axial Flow Compressors," ASME Paper No. 81-GT-154, 1981.

9. Takata, H., and Nagano, S. "Nonlinear Analysis of Rotating Stall," Journal of Engineering for Power, ASME Paper No. 72-GT-3, 1972.

10. Adamczyk, J. J. "Unsteady Fluid Dynamic Response of an Isolated Rotor with Distorted Inflow," United Aircraft Research Laboratories Paper No. 72-GD-3, 1972.

11. Pandolfi, M., and Colasurdo, G. "Numerical Investigation of the Generation and Development of Rotating Stall," ASME Paper No. 78-WA/GT-5, 1978.

12. Reddy, K. C., and Tsui, Y. Y. "Numerical Stability Analysis of a Compressor Model," AEDC-TR-82-16, 1982.

13. Erdos, J. I., Alzner, E., and McNally, W. "Numerical Solution of a Periodic Transonic Flow Through a Fan Stage," AIAA Journal, Vol. 15, No. 11, November 1977, pp. 1559-1568.

14. Reddy, K. C., and Nayani, S. N. "Compressor and Turbine Models - Numerical Stability and Other Aspects," AEDC-TR-85-5, 1985.

APPENDIX

THE DEVELOPMENT AND INCORPORATION OF UNSTEADY BLENDING FUNCTIONS

THE DEVELOPMENT AND INCORPORATION OF UNSTEADY BLENDING FUNCTIONS

During the development of the compressor code a spatial numerical oscillation in all the solution variables became distinctly apparent. This oscillation resembled a square wave in the axial direction, the solution being uniform in the tangential direction. The problem was subsequently traced to the manner in which the algebraic constraint equations that emulate the compressor blading were blended with the Euler continuum equations at the "leading edge" of the rotor and of the stator.

As given previously, the MacCormack explicit predictor-corrector algorithm was employed to solve the Euler equations exterior to the blade rows in the finite volume form:

PREDICTOR

$$\hat{G}^{N+1} = G^N - \frac{\omega\Delta t}{\forall}\{\sum_K F_K \cdot S_K^+ + \sum_K F_K^- \cdot S_K^- + W_s * \forall\} \quad \text{(A-1)}$$

CORRECTOR

$$G^{N+1} = \frac{1}{2\omega}\hat{G}^{N+1} + (1-\frac{1}{2\omega})\, G^N - \frac{\Delta t}{2\forall}\{\sum_K \hat{F}_K^+ \cdot S_K^+ + \sum_K \hat{F}_K \cdot S_K^- + W_s * \forall\} \quad \text{(A-2)}$$

where the source term W_s is an implicit source term in the sense that it is not explicitly calculated but rather is a consequence of the work input due to the rotor. It is non-zero only at the rotor nodes.

Equations (A-1) and (A-2) in their original form (i.e., for W_s not explicitly calculated) gave rise to the numerical oscillations.

In order to elucidate the cause of the oscillations, consider the approximation for the axial momentum equation as applied to a one dimensional control volume $\forall$ with an explicit source term W_s. In the predictor step,

$$\frac{\partial}{\partial t}(\rho A u)\Big|_i = \frac{-1}{\Delta x}\{\,\mathrm{imp}(i) - \mathrm{imp}(i-1) + W_s(i)\Delta x\} \qquad \text{(A-3)}$$

and in the corrector

$$\frac{\partial}{\partial t}(\rho A u)\Big|_i = \frac{-1}{\Delta x}\{\mathrm{imp}(i+1) - \mathrm{imp}(i) + W_s(i)\Delta x\} \qquad \text{(A-4)}$$

where imp(i) is the impulse function associated with node (i). Figure A-1 depicts the rotor nodes surrounded by duct nodes at each end.

The oscillation was instigated at node (i) in the corrector step due to the work input at node (i+1) that is absent at node (i). Referring to equation (A-3) and Figure A-1, the source term at $W_s(i)$ is zero such that the impulse functions at nodes (i-1) and (i) are equivalent in the steady state. In predicting the (i+1) node, the source term $W_s(i+1)$ accounts for the difference in impulse function between the (i+1) and (i) nodes, again in the steady state. This is the desired behavior.

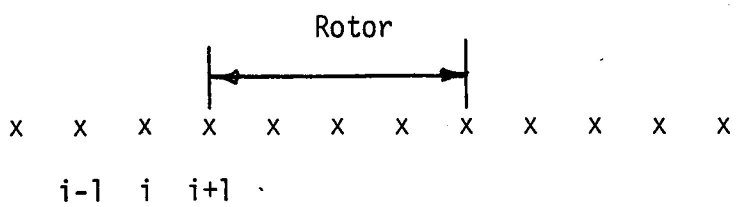

Figuer A-1. Rotor and Duct Node Interface.

Referring to the corrector sweep, as applied to node (i), equation (A-4) predicts that, in the steady state, the impulse functions at (i+1) and (i) are equivalent as $W_s(i)$ is zero exterior to the rotor. Thus, the problem was traced to the corrector step.

Upon combining equations (A-3) and (A-4) we have, in the steady state,

$$\mathrm{imp}(i+1) - \mathrm{imp}(i-1) = 2W_s(i)\Delta x \tag{A-5}$$

Since $W_s(i)$ is zero exterior to the rotor, the nodes (i+1) and (i-1) are coupled together--i.e., they have an equal impulse function. In addition, these nodes receive no source term input. Moving to the next node to the right, we see from equation (A-5) that

$$\mathrm{imp}(i+2) - \mathrm{imp}(i) = 2W_s(i+1)\Delta x \tag{A-6}$$

i.e., the node (i+2) receives twice the amount of intended source term input. This was precisely the observed result, i.e., a coupling between every other node in addition to amounts of applied work that were either zero or twice the appropriate amount. The problem was exacerbated by the fact that the model allows much of the total rotor work to take place at the leading edge when the blade is operating at high incidence, thereby yielding large values of W_s at the critical leading edge point.

The oscillation problem was alleviated by solving equation (A-3) for the implicit source term:

$$W_s(i) = \left(\frac{\rho Au^{N+1} - \rho Au^{N}}{\Delta t}\right)\Delta x + imp(i) - imp(i-1) \tag{A-7}$$

at the end of the predictor step and using it explicitly in equation (A-2) for the ith node during the corrector step. These source terms were implemented in order to conserve axial and tangential momentum, and energy at the rotor inlet; and to conserve axial and tangential momentum at the stator inlet.

VITA

Philip L. Andrew was born at Medina Memorial Hospital in Orleans County, New York on February 21, 1960. He received his secondary education from the Medina Central School System. Upon graduating in June 1978, he won a New York State Regents Scholarship and enrolled at the Rochester Institute of Technology, Rochester, New York. While studying at R.I.T., he participated in the cooperative education program, through which he was employed by the United States Department of Defense, the R.I.T. Research Corporation and the Harrison Radiator Division of the General Motors Corporation. After graduating with the baccalaureate degree in Mechanical Engineering in May, 1983, he enrolled at The University of Tennessee, Tullahoma, Tennessee where he held the position of Graduate Research Assistant under the direction of Dr. John E. Caruthers. Mr. Andrew received the Master of Science degree in Mechanical Engineering in December 1985 and subsequently commenced employment with the Aircraft Engine Business Group, General Electric Corporation, Cincinnati, Ohio.